27
7-8-76
Sent to NTIS

ORNL/TM-5441

Electrical and Optical Properties of the TTF-Halides

R. J. Warmack
T. A. Callcott

MASTER

OAK RIDGE NATIONAL LABORATORY

OPERATED BY UNION CARBIDE CORPORATION FOR THE ENERGY RESEARCH AND DEVELOPMENT ADMINISTRATION

DISCLAIMER

Printed in the United States of America. Available from
National Technical Information Service
U.S. Department of Commerce
5285 Port Royal Road, Springfield, Virginia 22161
Price: Printed Copy $5.00; Microfiche $2.25

ORNL/TM-5441

Contract No. W-7405-eng-26

HEALTH PHYSICS DIVISION

ELECTRICAL AND OPTICAL PROPERTIES OF THE TTF-HALIDES

R. J. Warmack and T. A. Callcott

Submitted by R. J. Warmack as a dissertation to the Graduate School of the University of Tennessee in partial fulfillment of the requirements for the degree of Doctor of Philosophy

JUNE 1976

OAK RIDGE NATIONAL LABORATORY
Oak Ridge, Tennessee 37830
operated by
UNION CARBIDE CORPORATION
for the
ENERGY RESEARCH AND DEVELOPMENT ADMINISTRATION

THIS PAGE

WAS INTENTIONALLY

LEFT BLANK

ACKNOWLEDGMENTS

The authors are indebted to Dr. J. L. Blankenship for his help in providing the conductivity measurement apparatus and assistance in computer programming, and to Dr. V. F. Raaen and C. R. Watson for growing the crystals used in this study. The authors also wish to express their thanks to Dr. C. K. Johnson for helpful discussions regarding crystal structures, and to Dr. H. C. Schweinler for his theoretical assistance and encouragement throughout the course of this work.

Special thanks go to Miss Anna L. McCray for typing this report.

Research was performed at the Oak Ridge National Laboratory under the sponsorship of the U. S. Energy Research and Development Administration under contract with the Union Carbide Corporation.

THIS PAGE

WAS INTENTIONALLY

LEFT BLANK

ABSTRACT

Recent interest in the highly conductive charge transfer organic crystals, particularly tetrathiofulvalene-tetracyanoquinodimethane (TTF-TCNQ), prompted us to investigate TTF-TCNQ and other systems. Results of conductivity measurements on TTF-TCNQ confirm results obtained by other authors.

TTF was found to combine with the halogens to form crystals with interesting electrical properties due to the segregated stacking of the TTF molecules. The monoclinic forms of TTF-I_n and TTF-Br_n ($n \sim 0.7$) have a high conductivity ($100\text{-}550\ (\Omega\text{-cm})^{-1}$) which is almost temperature independent for a very broad region near room temperature but display a thermally activated conductivity at low temperature. Unlike monoclinic TTF-Br_n, monoclinic TTF-I_n displays a strong hysteresis in its conductivity upon temperature cycling. The conductivity of the orthorhombic form of TTF-I_n ($n = 2$) is about five orders of magnitude lower than the monoclinic form at room temperature and is thermally activated over the entire temperature range.

Polarized single crystal optical reflectance measurements in the spectral region from 0.6 eV to 5 eV on the two crystalline forms of TTF-I_n were made. The reflection of light polarized along the conducting axis of the monoclinic crystals was typical of Drude-like free electron gas with the edge occurring at about 1.15 eV. Optical properties were determined by a Lorentzian oscillator fitting procedure. Results indicated that the majority of the visible spectrum can be attributed to TTF^+ transitions.

TABLE OF CONTENTS

LIST OF FIGURES

CHAPTER I

INTRODUCTION

Recently a great deal of research[1,2] has focused upon highly conductive charge transfer crystals. These crystals have several interesting and unique properties.

The crystal structure of these compounds consists of segregated stacks of π-electron rich planar molecules along which electrons move easily. Electrical[3,4] and optical[5] experiments have demonstrated the extreme anisotropy of these crystals. Band conduction is possible in these materials since the effective mean free path for electrons along the stacks of some compounds is longer than the unit cell dimensions.[6] Thus, these compounds can provide model systems in which one may study quasi-one-dimensional metallic behavior.

It has been suggested[7] that one-dimensional metals may be superconducting at much higher temperatures than ordinary three-dimensional metals. In fact, one group of observers has interpreted the conductivity of tetrathiofulvalene tetracyanoquinodimethane (TTF-TCNQ) in terms of BCS superconductivity.[7] This aroused considerable interest and controversy in the field. The interpretation may be valid if the intrinsic value of the conductivity of TTF-TCNQ is comparable to that observed in a very few, extraordinary samples of TTF-TCNQ.[6] These experimentally measured values have been questioned[8] and investigated.[4,9] The results tend to confirm the high conductivities, but, as yet, these have been observed in only one laboratory.[6] If the intrinsic conductivity is comparable to that observed in the vast majority of TTF-TCNQ crystals, then the conduction mechanism can be explained in terms of ordinary single particle electron scattering[6] or one of a number of other possible mechanisms.[10] Intensive research is underway at several laboratories which may help to clarify the controversy.

An effect competing with the conductivity in one-dimensional ordered metals is an instability of the lattice toward a distortion in which the molecules move closer to each other in pairs (Peierls distortion).[11,12] The spacial gaps between pairs create an energy gap which is seen by the electrons moving along the stacking axis, and the conduction is therefore thermally activated. The Peierls distortion has been confirmed in TTF-TCNQ through x-ray[13] and neutron scattering[14] experiments. Considerable effort has gone into stabilizing this distortion by introducing disorder[7] in the one-dimensional stacks. The flexibility of organic chemistry is certainly of great value in producing crystals with the desired structure and properties.

In TTF-TCNQ, charge is transferred[15] from the TTF stacks to the TCNQ stacks, and both stacks participate in conduction. With the development of the TTF-halides, it is possible to study the conduction of the TTF stacks alone. This should be of interest not only because of the simplification of single species conduction but also because the TTF molecules can be modified easily (e.g. selenium substitution for the sulfur) to introduce disorder in the TTF stacks. Three TTF-halide systems are described in this thesis which demonstrate the unusual properties of these materials.

In Chapter II several theoretical topics necessary in the analysis of the experimental data are briefly discussed. In Chapter III the experimental apparatus and procedures used in the conductivity and optical measurements are described. In Chapter IV we first summarize the results of a crystal structure determination of the TTF-halogen systems derived from the x-ray measurements of C. K. Johnson. We then describe and analyze our conductivity measurements made on TTF-TCNQ, TTF-Br_n, and on two crystalline forms of TTF-I_n. The final part of this chapter deals with the results of optical measurements on the two forms of TTF-I_n single crystals.

CHAPTER II

THEORY

Chemical Bonding[16]

The bonding between two electronegative elements results from a sharing of electrons to fill incomplete atomic shells and is termed covalent bonding. End to end overlap of "p-like" atomic orbitals forms a sigma bond while lateral overlap of these orbitals forms a pi bond. For example, consider a schematic of the bonding orbitals in ethylene ($H_2C = CH_2$).

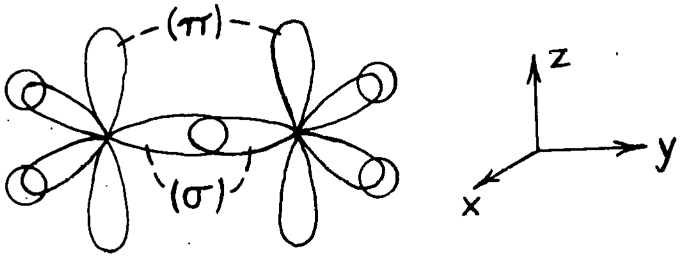

The triangular bonding arrangement of each carbon atom with the adjacent carbon and two hydrogen atoms is a result of hybridization of the s and p orbitals (sp^2 hybridization). A sigma bond is formed between the two carbon atoms due to orbital overlap along the y axis. The pi bond between the carbon atoms is due to the lateral overlap of the two "p-like" orbitals along the z axis. The sigma and pi terminology refers to the quantized orbital angular momentum about the internuclear axis in analogy with the angular momentum of atomic systems (i.e. $\ell = 0$ for s electrons, $\ell = 1$ for p electrons, etc.).

Conduction in Charge Transfer Crystals

In the highly conducting organic charge transfer crystals, an unusual crystal structure is seen. The molecules form one-dimensional stacks such that the plane of each molecule is parallel to that of the adjacent molecules in the stack. The interplanar distance is typically 3.2 Å to 3.6 Å so that significant π-orbital overlap occurs. If the stacking is uniform then one-dimensional electron energy bands are formed. Conduction is possible if a charge transfer partially empties or fills these bands.[17] For example, in TTF-TCNQ, the TTF stacks donate about 0.6 electrons per TTF to the TCNQ stacks.[15]

With one exception (hexamethyltetraselenofulvalene-TCNQ),[18] all charge transfer crystals at sufficiently low temperatures studied to date show conductivity of the form

$$\sigma = \sigma_o e^{-\Delta E/kT} , \tag{1}$$

where σ is the conductivity, σ_o is the high temperature limit of the conductivity, ΔE is the energy gap, k is Boltzmann's constant, and T is the absolute temperature. Such a temperature dependence arises from one of two conceptually different mechanisms. If a band picture is applicable (i.e., having an ordered system with sufficient electronic overlap) then the exponential temperature dependence of the conductivity is due to thermal activation of electrons from a filled energy band across an energy gap into an unfilled band where conduction may occur.

A small periodic distortion of the lattice can cause the bands to split and open band gaps. If a band splitting occurs in a metal having a partially filled conduction band such that the new bands formed are either filled or empty, then the metal will have been converted into a semiconductor. In the Peierls distortion where the periodicity of the lattice is doubled along one direction, the conduction band will be split in two. If the conduction band were originally half-filled then a metal to semiconductor transition would be seen. In materials where the band picture is not applicable due to disorder or very small electronic overlap, conductivity may be conventionally described in terms of a hopping mechanism in which electrons are thermally excited across an energy gap created by the spacial regions with little intermolecular overlap. Any distortion, periodic or not, which opens spacial gaps can lead to a thermally activated conductivity.

Some charge transfer complexes have been shown to have metallic-like conduction (i.e., an increase in the conductivity with a decrease in temperature).[11,19] In ordinary metals this is due to a change in electron-phonon scattering so that the conductivity is proportional to the inverse absolute temperature. In the highly conducting charge transfer crystals, this proportionality is not followed, and more complicated mechanisms may be needed to explain the conduction.[10]

The overlap along the directions perpendicular to the stacking axis is very small so that the conduction is considerably reduced. For example, the perpendicular conduction in TTF-TCNQ is about 10^{-2} to 10^{-3} times that of the high conductivity axis.[3,4] Thus these crystals are highly anisotropic.

Optical Models

The interaction of these crystals with light near the visible region can yield a great deal of information about the amount of charge transfer, the shifting and splitting of energy levels, and the polarizations of electronic transitions. This section discusses the optical models used in the analysis of the experimentally determined reflectivity. The following section on group theory discusses selection rules and polarizations of electronic transitions.

The classical theory of dispersion is due to Lorentz and Drude.[20] A quantum mechanical treatment of interband transitions gives results of exactly the same form as the Lorentz model. The classical model is derived by considering the electrons bound to the nucleus by a spring. A damping term is included to provide for an energy loss mechanism. When acted upon by an electric field which varies as $\exp(-i\omega t)$, the induced polarizability can easily be derived. The corresponding complex dielectric function is:

$$\hat{\epsilon}(\omega) = 1 + \frac{4\pi e^2}{m} \sum_j \frac{N_j}{(\omega_j^2 - \omega^2) - i\Gamma_j \omega} \tag{2}$$

where N_j is the density of electrons with resonant frequency ω_j, Γ_j is the damping term, m is the electronic mass, and e is the magnitude of electronic charge.

The corresponding quantum mechanical equation replaces N_j with Nf_j where N is the number of atoms per unit volume and where f_j is the oscillator strength given by

$$f_j = (2m\hbar\omega_j/\hbar^2)\,|x_{jo}|^2 \tag{3}$$

where $\hbar\omega_j = E_j - E_o$ (4)

is the energy difference between the ground and excited states, and

$$x_{jo} = \int \phi_j^* \, x \, \phi_o \, d\tau \tag{5}$$

is the matrix element of the coordinate vector along the polarization axis between the final and initial states. For free atoms the oscillator strength satisfies the sum rule

$$\sum_j f_j = 1 \tag{6}$$

in analogy with the classical formula

$$\sum_j N_j = N \ . \tag{7}$$

The real and imaginary parts of the dielectric function ($\hat{\epsilon} = \epsilon_1 + i\epsilon_2$) can be written as

$$\epsilon_1 = 1 + \frac{4\pi Ne^2}{m} \sum_i \frac{f_i(\omega_i^2 - \omega^2)}{(\omega_i^2 - \omega^2)^2 + \Gamma_i^2 \omega^2} \tag{8}$$

$$\epsilon_2 = \frac{4\pi Ne^2}{m} \sum_i \frac{f_i \Gamma_i \omega}{(\omega_i^2 - \omega^2)^2 + \Gamma_i^2 \omega^2} \ . \tag{9}$$

The first term in the expression for ϵ_1 should be replaced by an adjustable parameter ϵ_{core} if the tightly bound electrons are not included in the summation.

The Drude model is obtained by letting the restoring force go to zero in the Lorentz model. This model is applicable to the conduction electrons in a metal. Thus in the Drude model the resonant frequency is at $\omega = 0$ and the dielectric constant becomes

$$\epsilon_1 = \epsilon_{core} - \frac{\omega_p^2 \tau^2}{(1 + \omega^2 \tau^2)} \tag{10}$$

$$\epsilon_2 = \frac{\omega_p^2 \tau^2}{\omega(1 + \omega^2 \tau^2)} \tag{11}$$

where $\omega_p^2 = 4\pi Ne^2/m$ is the square of the plasma frequency and $\tau = \Gamma^{-1}$ is the mean free time between electron-phonon collisions.

Group Theory[21]

The application of group theory to the problem of the determination of transition probabilities between two states with wavefunctions ϕ_1 and ϕ_2 depends upon the evaluation of matrix elements of the form

$$\int \phi_1^* \vec{r}\, \phi_2 \, d\tau \quad . \tag{12}$$

The above matrix element uses the dipole moment operator since electric dipole transitions are usually much stronger than electric quadrupole, magnetic dipole, etc.

The integral (12) will vanish unless the integrand is totally symmetric and the two wavefunctions have a region of overlap. The latter requirement is not satisfied very well for $\sigma \leftrightarrow \pi$ transitions, thus these transitions are usually very weak. Both requirements can be met in certain $\sigma \rightarrow \sigma$ and $\pi \rightarrow \pi$ transitions. Group theory can easily tell us which transitions are allowed on the basis of symmetry.

Group theory can also tell us the symmetries of the molecular orbital wavefunctions. For example, the molecular orbitals of TTF belong to the point group D_{2h}. In this group a molecule must have three twofold axes of rotation (mutually perpendicular), three reflection planes (mutually perpendicular), and an inversion center, all of which leave the nuclear configuration unchanged. The energy levels of the molecular orbitals can be calculated from any of a number of computational schemes,[22] such as the Hückel, Pariser-Parr-Pople, etc.

The π-orbital energy levels of TTF, as calculated by the Hückel method,[23] are shown in Figure 1. Occupied levels for neutral TTF in the ground state are indicated by small circles. The polarizations of the allowed transitions between the six levels nearest the highest occupied molecular orbital are also indicated. These are easily determined by requiring the dipole moment operator to have the same symmetry as the product of the initial and final state wavefunctions.

For example, consider the $b_{1u} \rightarrow b_{3g}$ transition in neutral TTF. The ground state is totally symmetric (i.e., the square of the symmetry of each occupied molecular orbital is totally symmetric). The final state has the symmetry of the direct product $b_{1u} \times b_{3g}$. Since an electric dipole along the y axis has b_{2u} symmetry, then the product $\phi_1^* y \phi_2$ will be totally symmetric and the integral (12) will not vanish. The transitions in TTF$^+$ are similarly determined by assuming the highest occupied molecular orbital to be half filled.

Note that no $\pi \rightarrow \pi$ transitions can be excited by an electric field in the z direction (i.e., perpendicular to the molecular plane). These are forbidden by symmetry. The $\sigma \rightarrow \sigma$ transitions occur in the ultraviolet

ORNL DWG 75-16185

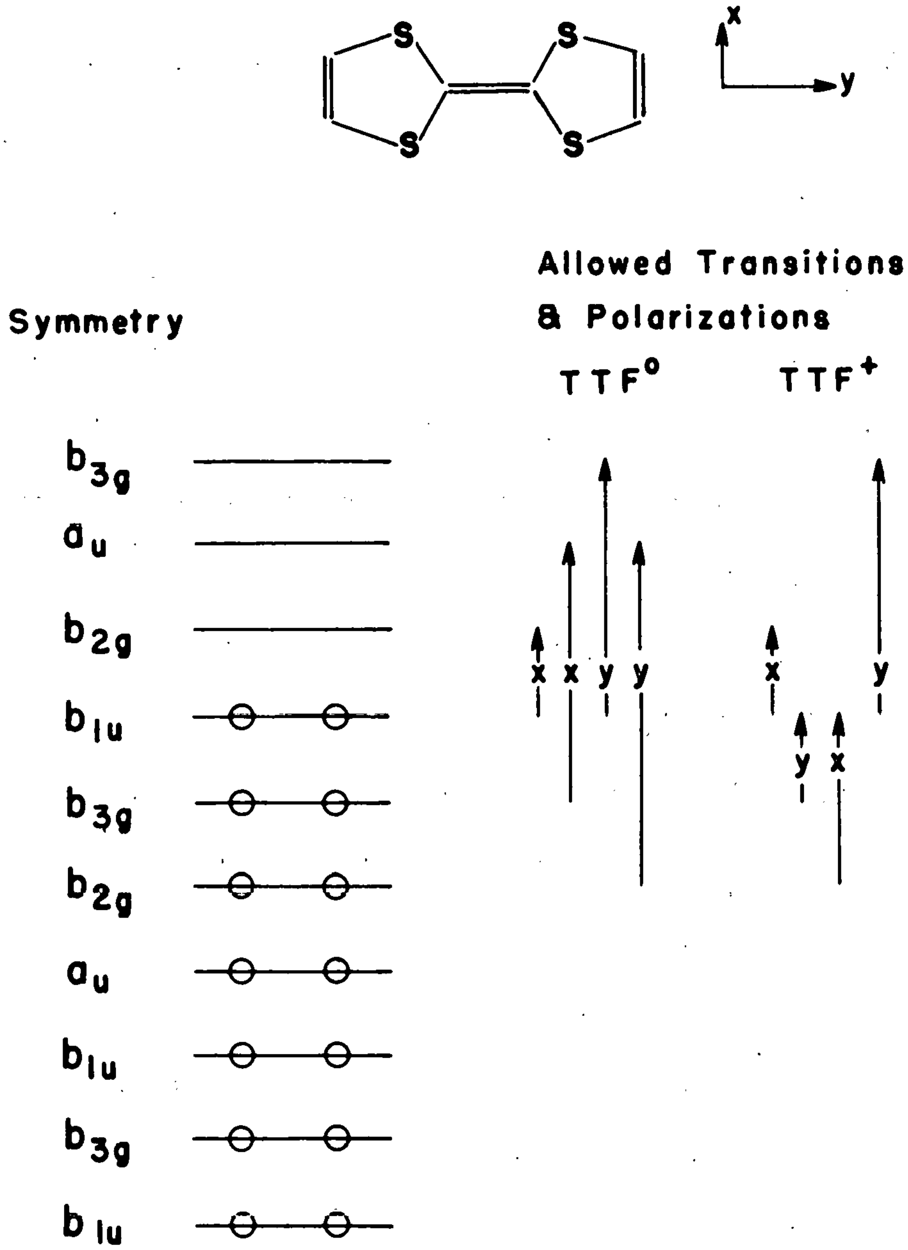

Figure 1. π-Orbital Energy Levels of TTF.

region typically, and the $\sigma \rightarrow \pi$ transitions are relatively weak due to the small overlap of the orbitals. Thus, little absorption is expected in the visible spectrum for z axis polarized light.

Forbidden transitions can become allowed by the coupling of vibration modes of the molecule to the electronic wavefunctions so that a totally symmetric integrand results. The strengths of these transitions, however, are typically 100 to 1000 times weaker than the transitions which are symmetrically allowed by considering the electronic wavefunctions alone. There are other ways in which forbidden transitions can become allowed, but these are usually very weak and are rarely observed.

CHAPTER III

EXPERIMENTAL APPARATUS AND PROCEDURE

Crystal Growth

All crystal samples were grown by V. F. Raaen and C. R. Watson of the Chemistry Division at Oak Ridge National Laboratory. Materials were either synthesized (e.g. TTF) and purified, or if commercially available, only purified (e.g. TCNQ). The purification procedures were fairly elaborate[6,27] in order to produce large single crystals with good conduction properties. The donor and acceptor compounds were then dissolved separately in acetonitrile (CH_3CN) and these two solutions were mixed (in the correct molar proportions). The resulting microcrystalline precipitate was then filtered, washed, and redissolved in hot CH_3CN. This solution was slowly cooled (~ 2 days) to room temperature and large charge transfer crystals resulted.

Another procedure was used for the TTF-halides because no good solvent was found for these charge transfer salts; thus recrystallization was impossible. Slow diffusion in a "U-tube" (shown below) was found to produce crystals of an acceptable size (1 - 5 mm). Needle-shaped crystals formed in the glass wool in the TTF chamber while smaller flat crystals formed in the "U-tube" below.

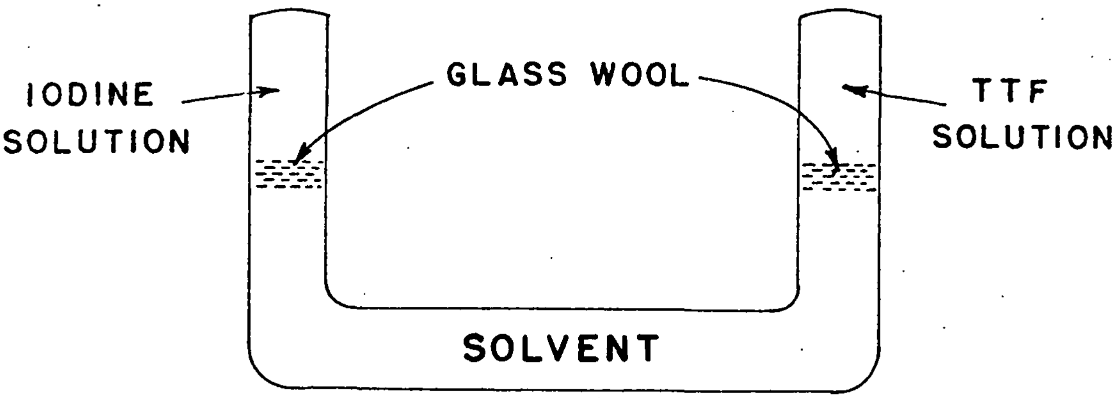

<u>Conductivity Measurement Apparatus</u>

In order to measure the dc conductivity as a function of temperature, cryogenic apparatus was needed to obtain control of temperature of the samples from room temperature to liquid nitrogen temperature. Suitable apparatus[24] was found in the Instrumentation and Controls Division of Oak Ridge National Laboratory. The equipment had been designed for Hall effect measurements on semiconductors and was ideal for various conductivity experiments with only a few small modifications.

Figure 2 shows the internal design of the cryostat which was a modification of a Sulfrian Cryogenics Model 64445. The sample chamber could be evacuated and backfilled with either nitrogen or helium mixing gas to provide thermal contact with the cold reservoirs.

The sample chamber was machined out of solid copper and is shown in Figure 3. Platinum and germanium resistance thermometers

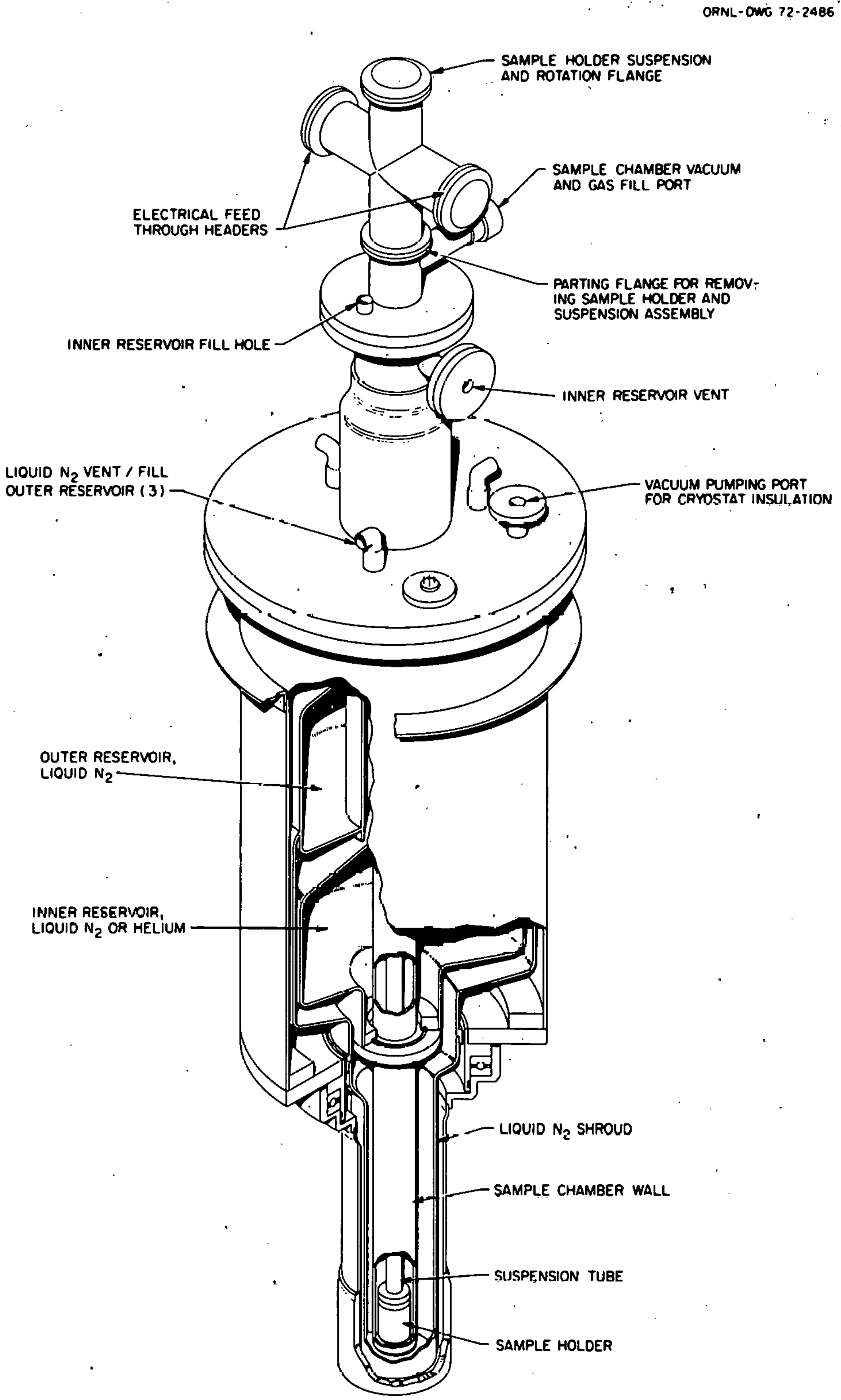

Figure 2. Cutaway Drawing of Cryostat.

ORNL DWG 75-16183

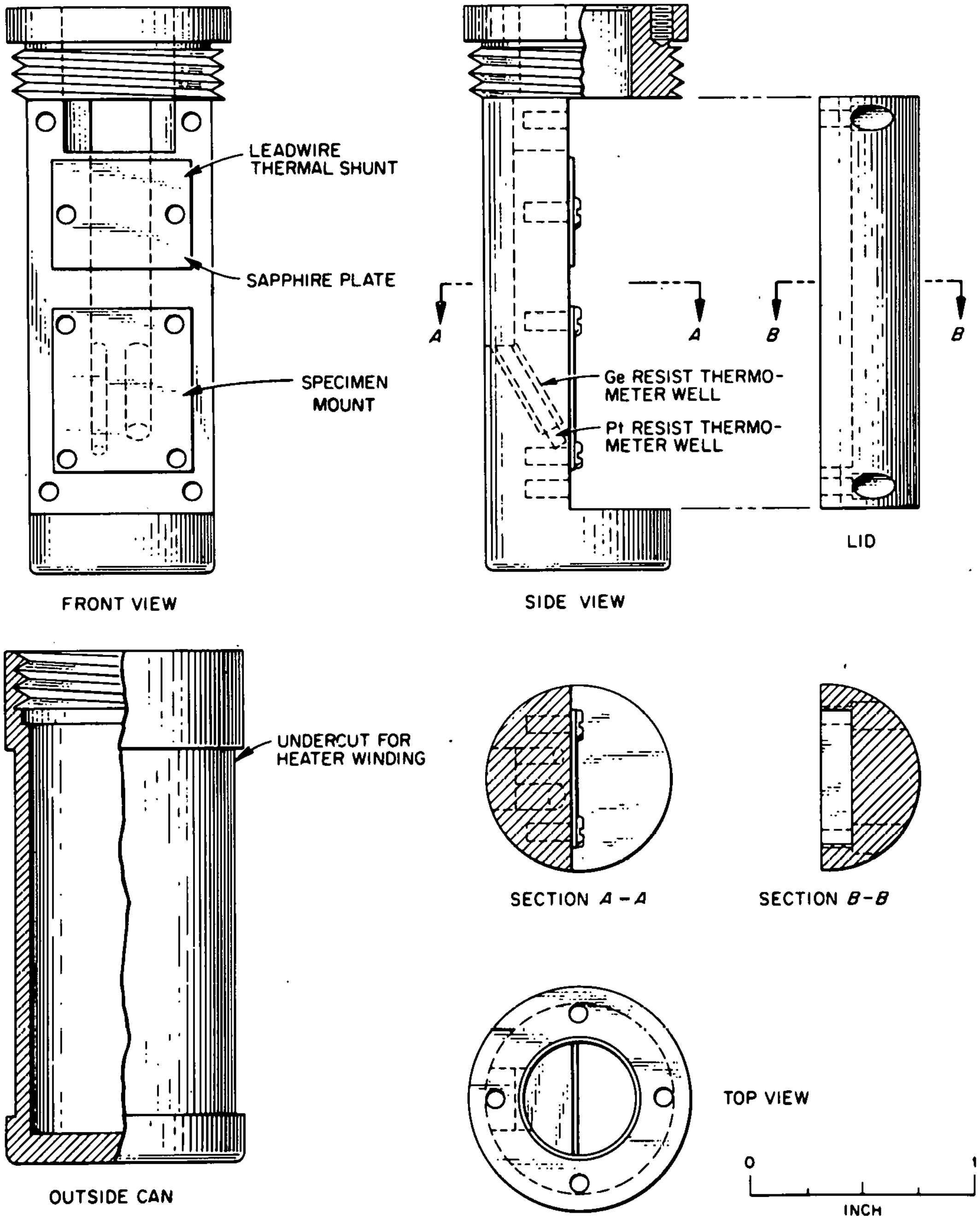

Figure 3. Sample Chamber Assembly.

were buried directly underneath the sample and a copper-constantan thermocouple was attached to the lead wire thermal shunt. The resistance thermometers were connected to a temperature control system made by Honeywell, Inc. The resistance was first converted into a voltage which was displayed on an Electronic 16 Continuous Balance Potentiometer and Recorder. A particular resistance (temperature) could be selected on the recorder and an error signal would be sensed by an Electro-Volt Control Unit if the selected resistance did not correspond with the thermometer resistance. The output of the Control Unit then controlled the power to a heater which was wrapped around the outside of the sample chamber.

Current to the sample was supplied by an isolated 45 volt battery in series with a high resistance so that the current could be selected from 10^{-3} amp. to 10^{-8} amp. Thermoelectric effects could be averaged out by taking conductivity measurements for both directions of current flow. Accurate current measurement was provided by measuring the voltage across a precision resistor in series with the current circuit.

Sample current, sample voltage, thermometer resistance, and thermocouple voltage were measured by a Hewlett-Packard Model 3490 A Digital Voltmeter. This instrument had an input impedance of greater than 10^{10} ohms so that sample resistances below about 10^{8} ohms had a negligible load correction.

Data was recorded by interfacing the digital voltmeter to a teletypewriter through a Hewlett-Packard Model 2570A Coupler/Controller. This provided proper formatting for the data punched on paper tape which was reduced by means of a PDP-10 computer.

The samples themselves were prepared as follows. Crystals were selected visually to conform to the ideal - a rectangular parallelepiped. The conductivity along the long axis of the needle-shaped crystals could be measured quite simply by attaching current leads near each end of the sample and measuring the voltage differences of two points situated along the length of the sample. Since these crystals were extremely anisotropic, care was taken to locate these voltage probes as far away from the current leads as possible in order for the current flow to be uniform throughout the cross section in the critical region (between the voltage probes). Appendix I details the anomalous conductivity results possible if this condition is not satisfied.

Figure 4 shows a diagram of the conductivity mount with a needle-shaped specimen attached. Two types of printed circuit boards were made to hold samples of lengths greater than 3.5 mm and greater than 6 mm. Some samples used were as small as one millimeter long but the essential arrangement is the same as shown in Figure 4. One mil gold wires were stretched across the board and were fastened by applying silver paint or silver epoxy. The sample was laid upon the gold wires

ORNL DWG 75-16193

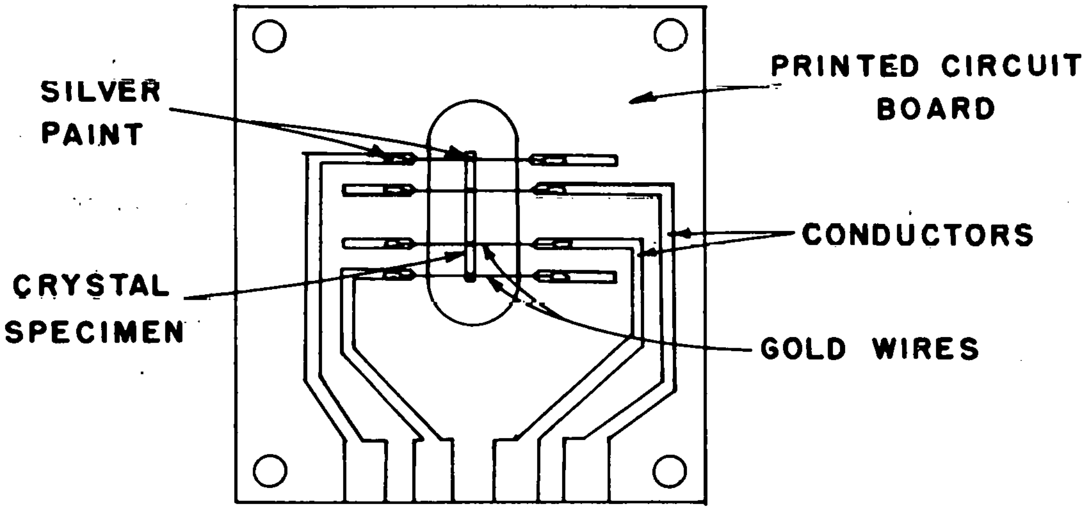

Figure 4. Conductivity Sample Mount.

and contacts were carefully made under a microscope. It was found convenient to use a small glass fiber pulled from a heated glass rod to apply the silver paint (Dupont No. 4817 or No. 7941) connecting the sample with the gold wires. Voltage contacts were made as small as possible to avoid disturbing the potential field in the sample and to allow accurate measurement of the length between voltage probes. Dimensions were measured using a calibrated, movable crosshair eyepiece in the microscope.

The silver paint, by itself, was found to produce a relatively poor contact with any of the TTF-halides. This may have been due to a chemical reaction of the halide with the silver. Therefore, thin strips of gold were evaporated upon the samples before the silver paint was applied. Masking was done by using small pieces of sheet metal. The silver paint applied to the gold areas provided good, stable contacts.

A different arrangement was needed to measure the conductivity of the TTF-I_2 platelets. These had typical dimensions of 0.5x0.5x0.05 mm and the conducting axis was along the thin dimension. Figure 5 is a schematic of the arrangement with the edge of the sample showing. Gold was evaporated on both faces of the sample to provide good uniform electrical contact. A shadow cast by a two mil wire during evaporation separated the voltage and current contacts. The edges of the sample were then cleaved to insure that any gold deposited there

ORNL-DWG 75-6260

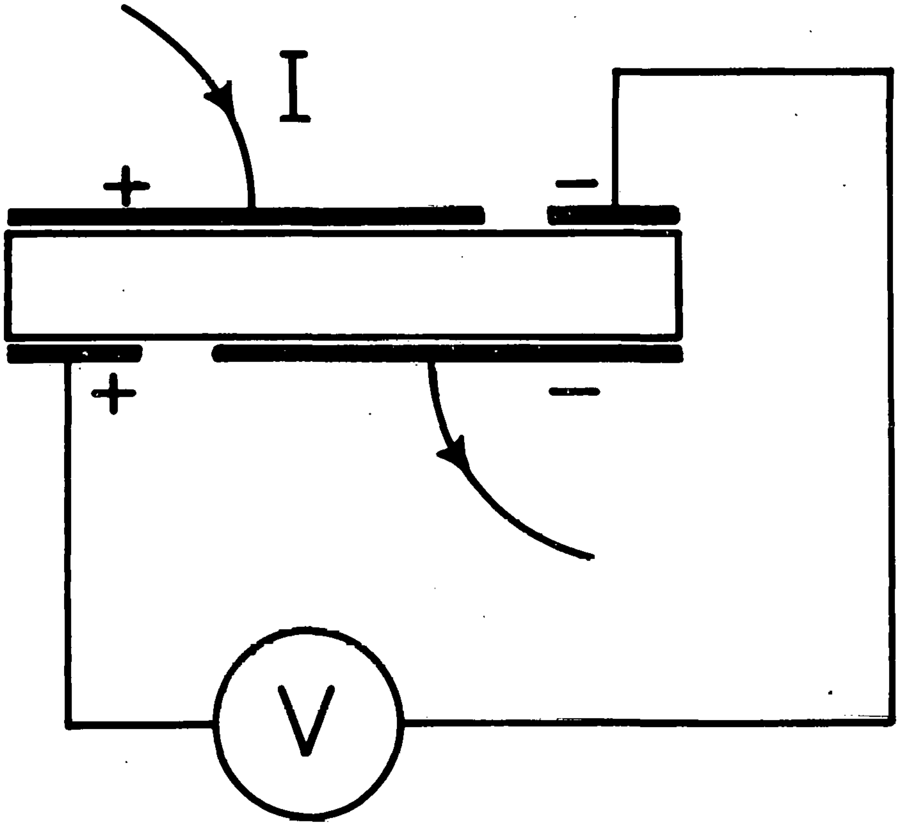

Figure 5. Schematic Diagram of the Conductivity Measurement for Orthorhombic TTF-I_n.

would be removed. With this arrangement the current flow concentrated in the overlap region between the current contacts since the conductivity along the two perpendicular directions was found to be two orders of magnitude lower than that along the thin dimension. Thus the voltage contacts were electrically "close" (i.e., nearly the same potential) to the current contact on the opposite face of the sample.

Other configurations of electrical contacts were employed to measure conductivities along the other principal axes of these crystals. The most useful was that due to Montgomery[25] in which point contacts are made at each of the four corners of one face of a rectangular parallelepiped. Current is passed between adjacent pairs of contacts and voltage is measured between the other pair of contacts. Results can be analyzed to give conductivities for both axes of the rectangle. In practice, however, the difficulties involving finding a perfect rectangular surface and securing good point contacts on these small organic crystals restrict this method's usefulness. Nevertheless, good estimates of the perpendicular conductivities can be made using this method.

Conductivity Measurement Procedure

The sample is placed in the sample chamber and lowered into the cryostat. Sample current is increased to get reasonable value of voltage developed in sample but low enough to keep the power well below one microwatt. Voltage and current leads are permuted to check for anomalous current patterns in the sample. A data header is punched on paper tape which includes identification and the dimensions of the sample.

The sample chamber is evacuated and filled with helium gas to about 5 - 10 lb./in.^{2} above atmospheric pressure. The inner and outer reservoirs and the thermocouple reference dewar are filled with liquid nitrogen. When using liquid nitrogen as a coolant the temperature descent is so slow ($<$ 1°K/min.) that the temperature controller is not employed and data is taken without stabilizing the sample temperature.

When the desire temperature is reached a data-taking sequence is begun. Thermocouple voltage, current shunt voltage, sample voltage, reversed current and voltage, and resistance thermometer value are recorded by manual switching. Above 20°K the platinum thermometer is used. The output of the DVM is automatically formatted and punched on paper tape. Other values are punched manually whenever the current shunt or the resistance thermometer conditioner scale are changed.

When a temperature of 80°K to 90°K is reached and lower temperatures are desired, liquid nitrogen cooling is replaced by liquid helium. The inner reservoir is emptied and the sample chamber evacuated. The inner reservoir is then filled with liquid helium. Pressure in the sample chamber is increased to about 20 in. Hg vacuum and the sample begins to cool rapidly. For these temperatures the automatic temperature controller is used to stabilize the temperature at any desired set point. Adjustment of the controller must be made to provide for the changing specific heat of the copper sample holder.

To check for any hysteresis in the conductivity curve a heating cycle is performed next. The reservoirs are emptied and the sample heater is turned on to give the desired rate of temperature change.

When the experiment is completed, the paper tape is read into a computer and the reduced data is typed out which includes the thermocouple and resistance temperatures and the conductivities (see Appendix II).

Reflectivity Measurement Apparatus

Since the crystal samples were quite small, special apparatus was designed to measure the specular reflectance of single crystal samples as a function of wavelength. One could mask off the unwanted portion of a collimated beam of light but problems would be encountered such as signal intensity and scattered light. A better solution is to focus the light to a spot as small as the sample itself.

Several methods to focus the light were tried. A Leitz microscope fitted with a monochromatic light source was used initially but severe problems were encountered with scattered light. Also, since the polarizer had to be placed just above the sample in both incident and reflected beams, some intensity was lost due to elliptical polarization of the reflected beam, and this possibly distorted the reflectance curve. In any case the instrument could not be used below about 4000 Å due to the wavelength cutoff of the glass optics.

Another method, which proved to be much more successful, used a single quartz lens to image the exit slit of the monochromator onto the sample. This allowed the use of wavelengths as small as 2000 Å and the polarizer[26] could be placed such that only the incident beam was affected. A problem inherent in a refractive system is the variation in the index of refraction with wavelength. Frequent repositioning of the sample was needed to compensate for changes in the focal point.

A reflective focusing system was designed such that the focal point remains fixed with a variation in wavelength. A sketch of the focusing assembly appears in Figure 6. Light from the monochromator enters through the aperture plate and is reflected from the small convex mirror onto the large concave mirror which focuses the light onto the sample. The system was actually designed for maximum light throughput for a 0.5 m Seya-type monochromator but a Jarrell Ash Model 82-410 monochromator was used in this experiment. The mirrors were coated with evaporated aluminum followed immediately by an overcoat of MgF_2 220 Å thick to prevent oxidation. The distance between

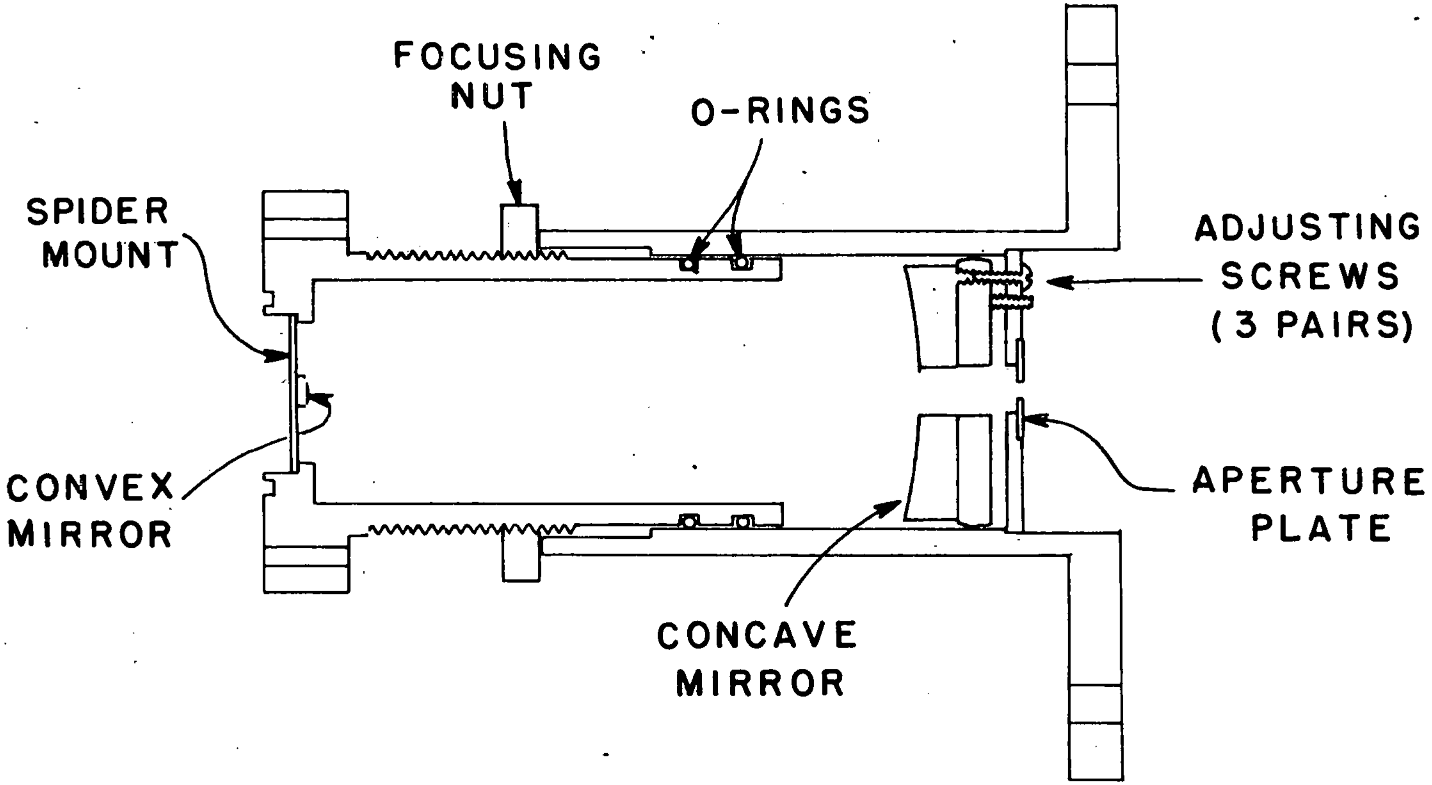

Figure 6. Cutaway Drawing of the Focusing Assembly

the mirrors was adjustable to provide proper focusing. The system could be evacuated so that the vacuum ultraviolet region could be studied if desired.

Figure 7 shows a schematic of the entire reflectance apparatus. Source lamps of tungsten for visible and infrared and xenon for ultraviolet were used in an Oriel lamp housing. A light chopper was used in conjunction with a lock-in amplifier for the infrared detector. Various optical filters were placed in front of the monochromator to insure no scattered or second order light passed through the system. Three gratings with blaze wavelengths of 3000 Å, 6000 Å, or 10,000 Å were used in the monochromator. The monochromatic light then passed through the focusing system which was attached to the high vacuum station where the sample and polarizer were housed. The polarizer (a one-inch Glan prism) was mounted on ball bearings and a vacuum manipulator was attached so that the prism could be rotated 90°. The sample and reference mirror (a calibrated MgF_2 overcoated aluminum mirror) were mounted upon a copper block fastened to an Air Products Heli-Tran refrigerator. The reflected light exited through another vacuum port to the detector (either a photomultiplier or a lead sulfide photoconductor). Both entrance and exit windows on the high vacuum station were MgF_2 to pass the ultraviolet light.

Steps were taken to avoid scattered light in the sample chamber. An aperture plate in front of the sample for the incident light and a cone-

ORNL DWG 75-16184

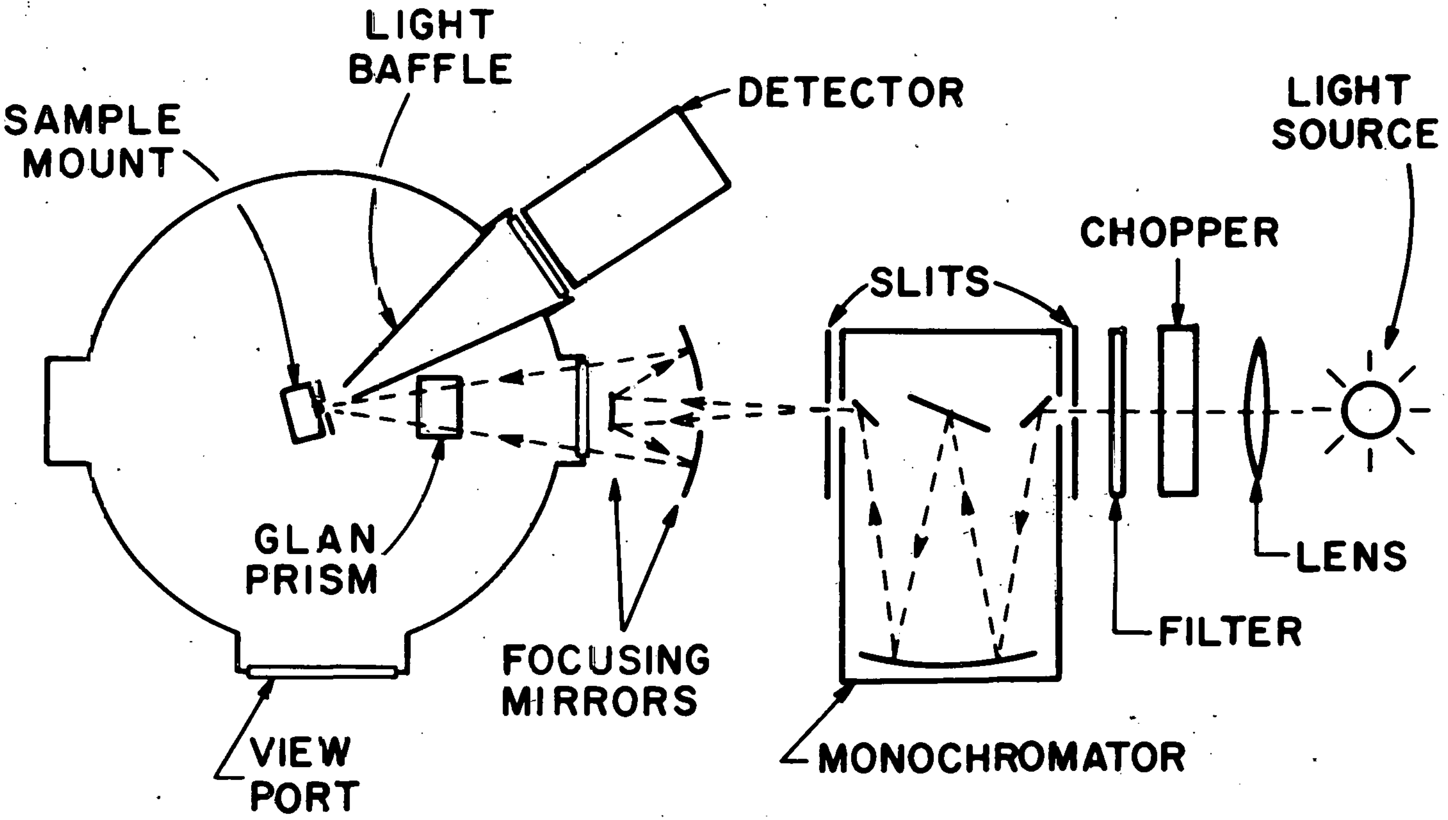

Figure 7. Schematic Diagram of the Reflectance Apparatus.

shaped aperture plate for the exit light were used. Both sample and mirror were mounted immediately behind a pair of machined copper slits which were blackened by heating in air. Other places where stray light could enter the apparatus were covered by black optical cloth.

Reflectivity Measurement Procedure

A crystal is selected which has a smooth flat face and is fastened to the sample holder with silver paint or silicone grease so that the crystal surface is as nearly parallel as possible to the surface of the holder. The sample assembly is lowered into the vacuum chamber and adjusted so that the light focused upon the sample is reflected to the detector.

For visible measurements (3500 Å to 9000 Å) the tungsten lamp is used with a photomultiplier detector. The 6000 Å blaze grating is fitted into the monochromator. The amplified output of the photomultiplier is recorded on a strip chart recorder as the monochromator scans through the desired range. During the scan, optical low-pass filters are inserted at the monochromator to insure that no second order light is detected. Long-pass filters are particularly important near the long wavelength end of the scan since the output of the photomultiplier diminishes greatly in this region. When the scan is completed, a check is made to detect any variation in the lamp output. The sample holder is lowered so that the reference mirror comes into position and is adjusted so that the reflected beam falls upon the detector. The same scan is repeated.

For the ultraviolet region (2300 Å to 4500 Å), the tungsten lamp is replaced with the xenon lamp and the 3000 Å blaze grating is fitted into the monochromator. The scans are performed as before using band pass filters to insure that the proper wavelengths are detected.

In the infrared region (8000 Å to 20,000 Å), the 10,000 Å blaze grating and the tungsten lamp are used. The detector is a lead sulfide photoconductor with 2 mm square sensitive area. A glass lens is fitted at the exit port of the vacuum chamber in order to focus the light onto the detector. A lock-in amplifier is used in conjunction with a light chopper. The scans are performed as before using low pass filters.

The reflectance at various points along each scan is calculated according to

$$R = \frac{I}{I_o} \cdot R_{Al} \qquad (13)$$

where R is the reflectance, I is the intensity of the sample reflected beam, I_o is the intensity of the reference mirror beam, and R_{Al} is the reflectance of the reference mirror. The overlap regions for the three scans can serve as a check on the accuracy of the measured reflectance.

CHAPTER IV

RESULTS AND ANALYSES

The results of our experimental study on TTF-TCNQ and three forms of the TTF-halides are presented in this chapter. The results of our TTF-TCNQ study will not be emphasized, however, since they only confirm previous results obtained by other authors.[6] In order to better understand the analyses of the TTF-halides, the TTF-I_n crystal structures are first discussed. The results of the optical experiments are then presented and analyzed. Information on charge transfer obtained from the crystal structure and optical studies is used to help interpret the results of the conductivity experiments on the TTF-halides.

Crystal Structure of TTF-I_n

The three dimensional crystal structures of the two forms of TTF-I_n have been determined[27] by C. K. Johnson of the Chemistry Division at Oak Ridge National Laboratory. The orthorhombic form appears as small platelets, and the monoclinic form appears as long thin needles.

In the orthorhombic form a stoichiometry determination gives $n = 2$. A projected view of the structure appears in Figure 8. The TTF molecules form stacks such that the plane of each TTF molecule is approximately perpendicular to the stacking axis. Note that the thermal

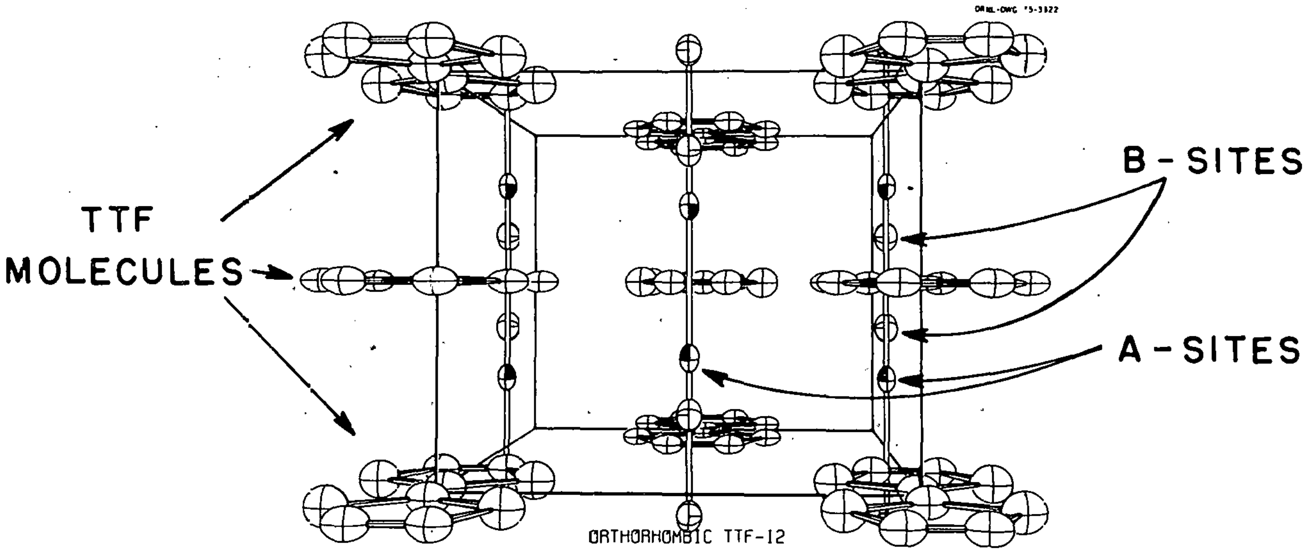

Figure 8. Projected View of the Orthorhombic TTF-I_n Crystal Structure.

ellipsoids for the atoms in alternate TTF molecules are broadened. This suggests that the planes of alternate TTF molecules are rotated by small amounts (~ 10°) about their low inertial axes.

The iodine atoms form columns parallel to the TTF stacking axis. Each iodine occupies one of two positions (termed A and B), which are approximately 1 Å apart. The bond lengths and bending angle are indicative of the I_3^- species but this does not correspond with the observed occupancy figures - position A, 79%; position B 21% (i.e. occupancy ratio A:B ≅ 4:1. Therefore the iodine columns must contain some monomer or dimer species to increase position A occupancy. Species longer than the trimer are bent[28] by 90° and are not expected to be present. A 1:1 ratio of trimer and monomer gives an occupancy ratio of A:B = 3:1. A closer correspondence to the observed occupancy ratio is given by repeated units of trimer-monomer-trimer-monomer-dimer (TMTMD) which gives the ratio of A:B = 4:1. Other combinations of poly-iodide species give occupancy ratios which fall outside of experimental error.

The projected view of the monoclinic structure is shown in Figure 9. The stoichiometry of the crystal sample studied gave n = 0.7079. This crystal is isostructural with monoclinic TTF-Br_n which has been shown[29] to have a variable stoichiometry of $0.7 < n < 0.8$. The TTF molecules form stacks with the plane of each TTF approximately pendicular to the stacking axis. Adjacent stacks are rotated 90° about the stacking axis. Within

ORNL-DWG 75-3321

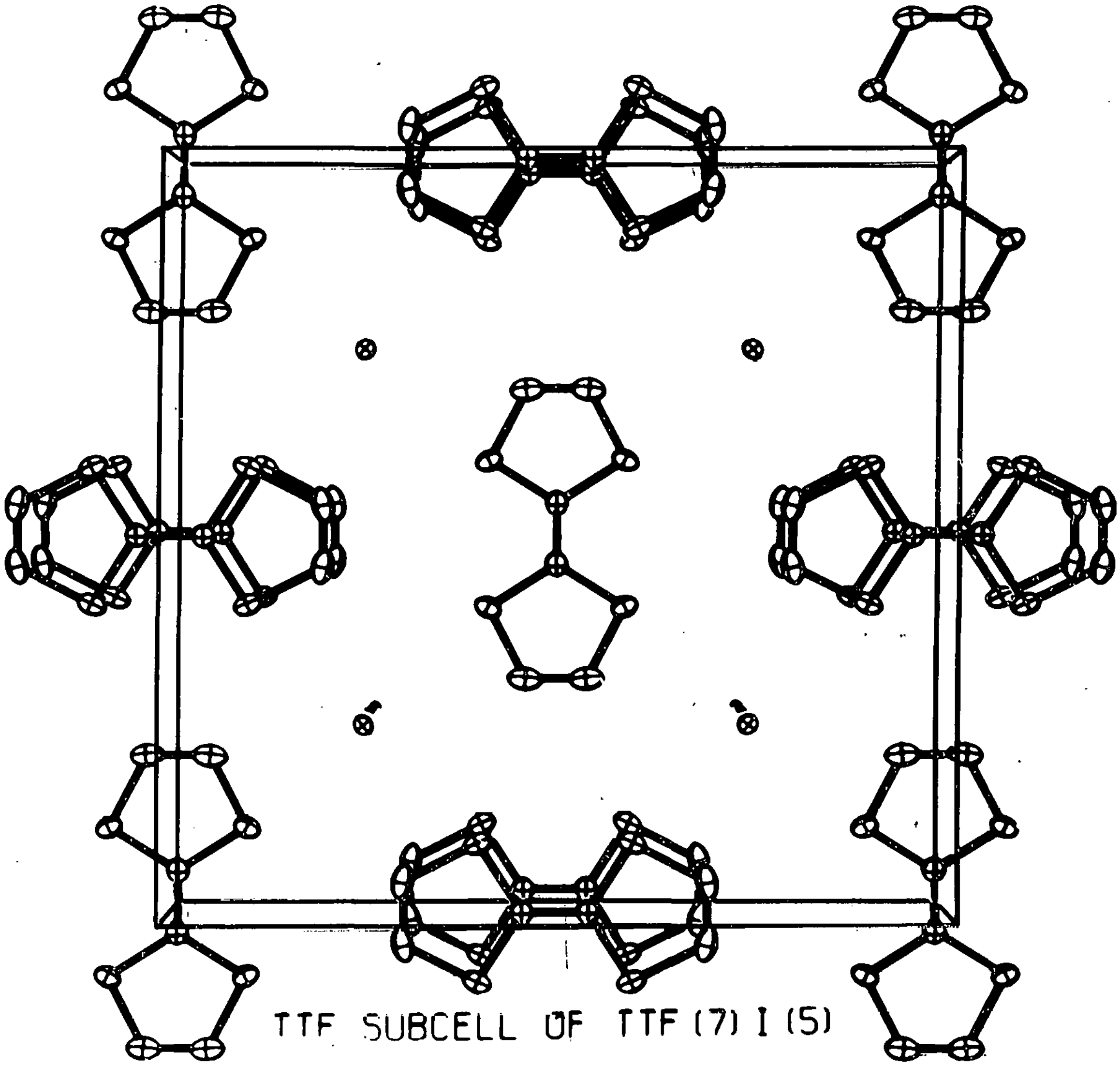

Figure 9. Projected View of the Monoclinic TTF-I_n Crystal Structure.

each stack some rotational distortion is present so that the adjacent TTF molecules are rotated by as much as 10° about the stacking axis. The iodine forms columns with a spacing between iodine ions of about 5 Å, controlled by the stoichiometry. This crystal structure is unusual because the TTF and iodine form two, separate, incommensurate lattices.

Optical Properties

The room temperature reflectance of monoclinic TTF-I_n is shown in Figure 10. The spectra show the expected anisotropic behavior. Along the stacking axis (z) the reflectance displays a plasma edge corresponding to intrachain charge transfer, with reflectance rising from a minimum of less than 1% at 1.5 eV to a value of 55% at 0.7 eV. Little structure is noted in the visible and the reflectance slowly rises toward the ultraviolet. Perpendicular to the stacking axis the plasma edge is not seen and much structure is evident in the visible region.

The difference in reflectance in the overlap region between the visible and infrared spectra along the stacking axis is due to light leakage from the long wavelength region (to which the infrared detector is very sensitive) which raises the minimum in reflectance. This leakage was confirmed using a slice of silicon, which is quite opaque to wavelengths below 9000 Å, to act as a low pass filter.

ORNL DWG 75-16187

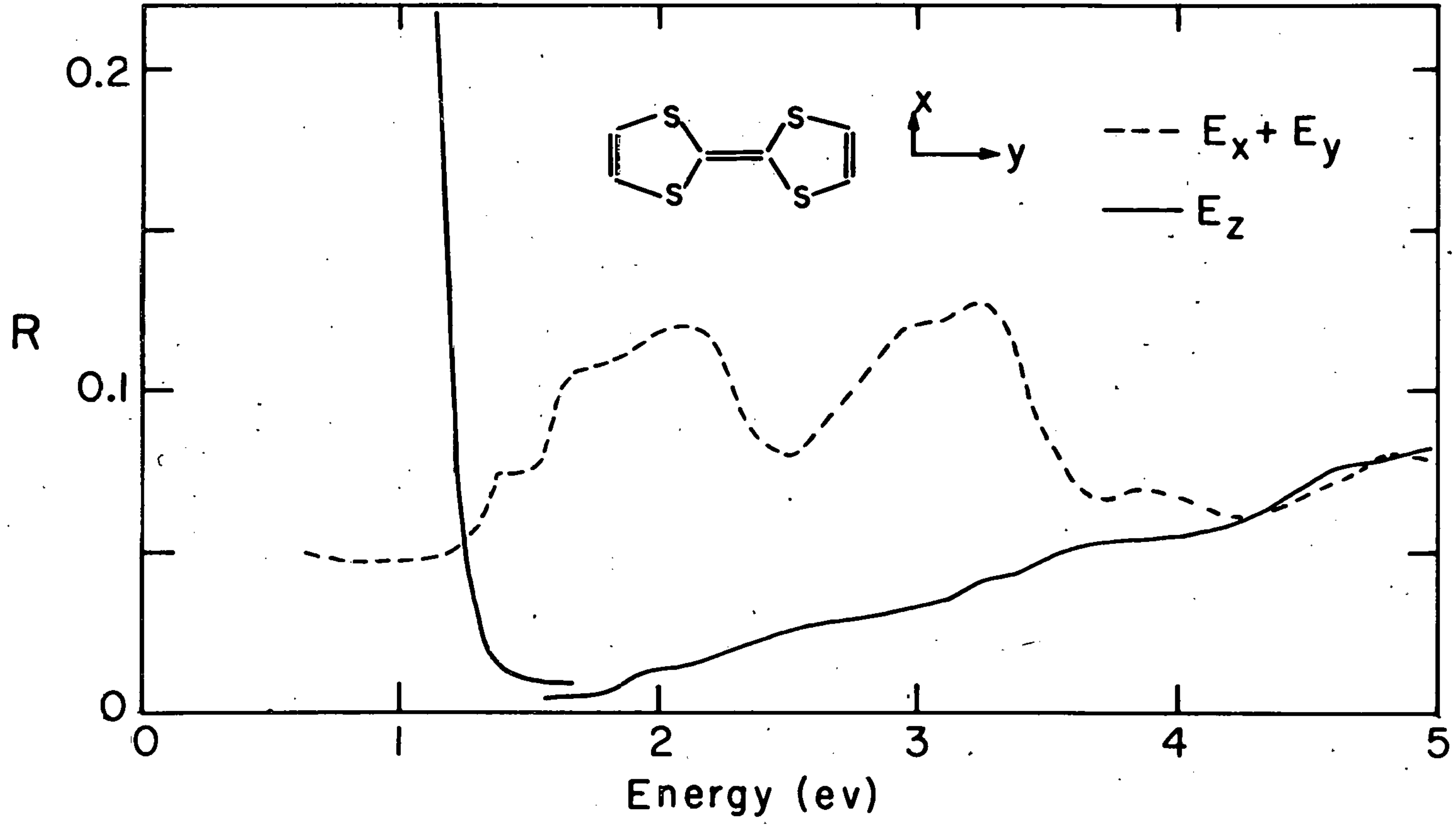

Figure 10. Reflectance ot Monoclinic TTF-I_n.

Another experimental difficulty is that some of the light which falls on the sample has components of the electric vector that are not parallel to the surface of the sample. This is due to the non-normal incidence of the light as a result of the convergence of the light beam and the rotation of the sample. The convergence of the light affects the reflection along the stacking axis since about 5% of the intensity of the electric vector is polarized in the plane of the TTF molecules (perpendicular to the stacking axis). The dominant effect would be seen where the difference in the two polarizations is the greatest, i.e., the long wavelength reflectance should be slightly greater ($\sim 1\%$) along the stacking axis. Perpendicular to the stacking axis no effect should be seen due to the fact that crystal structure is similar along the two perpendicular axes.

The reflectance data along the stacking axis were fitted to the Drude model using a nonlinear least-squares computer program to determine parameter values. The best fit was obtained with $\epsilon_{core} = 1.315$, $\omega_p = 1.983 \times 10^{15}$ sec^{-1} ($\hbar\omega_p = 1.305$ eV) and $\tau = 2.573 \times 10^{-15}$ sec. The reflectance calculated from these values is compared with the experimental reflectance in Figure 11. The dc conductivity ($\omega_p^2 \tau / 4\pi$) calculated using these parameters is 894 $(\Omega - \text{cm})^{-1}$ in good agreement with the measured dc value at room temperature.

It should be noted the Drude model fit is not unique. The data may be equally well fitted by the Lorentz model in which a strong

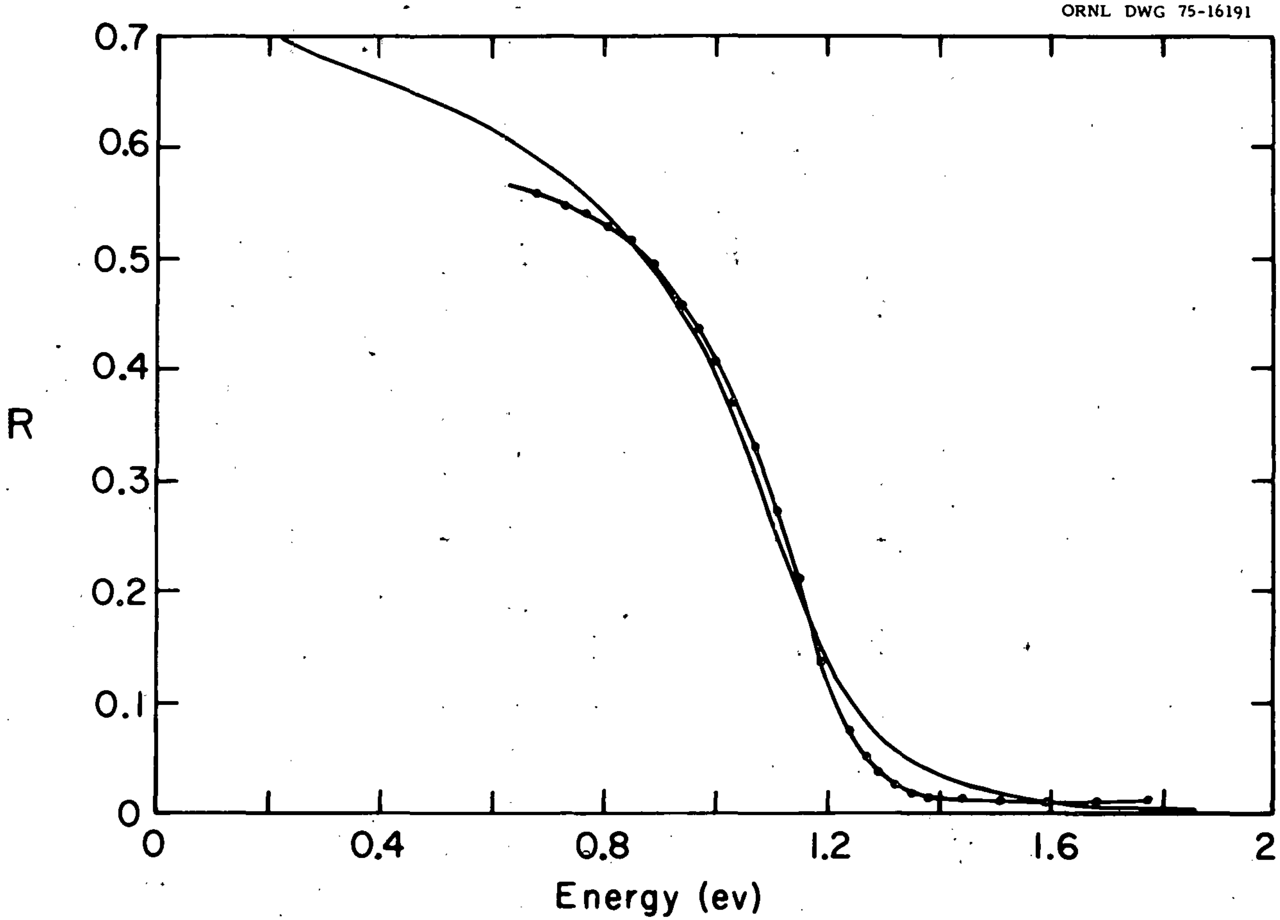

Figure 11. Reflectance of monoclinic TTF-I_n Along its Stacking Axis Compared with a Drude Fit.

Experimental points are shown as solid circles.

electronic transition is located near the plasma edge. The best fit to the experimental data placed the oscillator at $\hbar\omega = 0.5$ eV. The basic difference between the Drude model and the Lorentz model appears at very long wavelengths where the reflectance from the Lorentz model falls with increasing wavelength. Unfortunately, the range of wavelengths covered in this experiment does not permit a clear distinction to be made between the two models.

The absence of any structure in the visible is due to the forbidden nature of the low energy electronic transitions ($\pi \rightarrow \pi$) perpendicular to the plane of the TTF molecules. The iodine atoms are well separated (~ 5 Å) and no strong transitions are expected in this region for neutral or singly charged iodine.[30]

The reflectance along the stacking axis was also measured at liquid nitrogen temperature. The effect of lowering the temperature was to shift the plasma edge about 0.05 eV to higher energy. This shift is typical of other charge transfer crystals.[31] No detailed analysis is presented here since experimental difficulties with the vacuum system made some of the reflectance data suspect. However, all the major structure was very similar to the room temperature data.

The reflectance of orthorhombic TTF-I_n was measured for the large face of the crystal for which the plane of the TTF molecules is approximately parallel. Also, since the TTF molecules are all aligned, the transitions for the two in-plane axes of TTF can be resolved (see Figure 12). Note that the major structure of the monoclinic reflectance (perpendicular to its stacking axis) is very similar to the resolved orthorhombic structure.

The effect of the non-normal incidence of the light beam was to introduce a small component of the transitions along the stacking axis. This contribution amounted to about 5% for vertically polarized light (along the x axis of the TTF molecules) and about 10% for horizontally polarized light (along the y axis of the TTF molecules). Thus no transitions along the stacking axis would be seen in these data unless they were very strong.

The reflectances of the two polarizations of orthorhombic TTF-I_n and the perpendicular polarization for monoclinic TTF-I_n were fitted with a sum of Lorentzian oscillators. The procedure was to guess values of the oscillator parameters, calculate ϵ_1 and ϵ_2 according to equations (8) and (9), and calculate[19] the reflectance according to

$$R = \frac{|\epsilon| + 1 - \sqrt{2(|\epsilon| + \epsilon_1)}}{|\epsilon| + 1 - \sqrt{2(|\epsilon| + \epsilon_1)}} \,, \tag{14}$$

where

$$|\epsilon| = \sqrt{\epsilon_1^{\,2} + \epsilon_2^{\,2}} \quad . \tag{15}$$

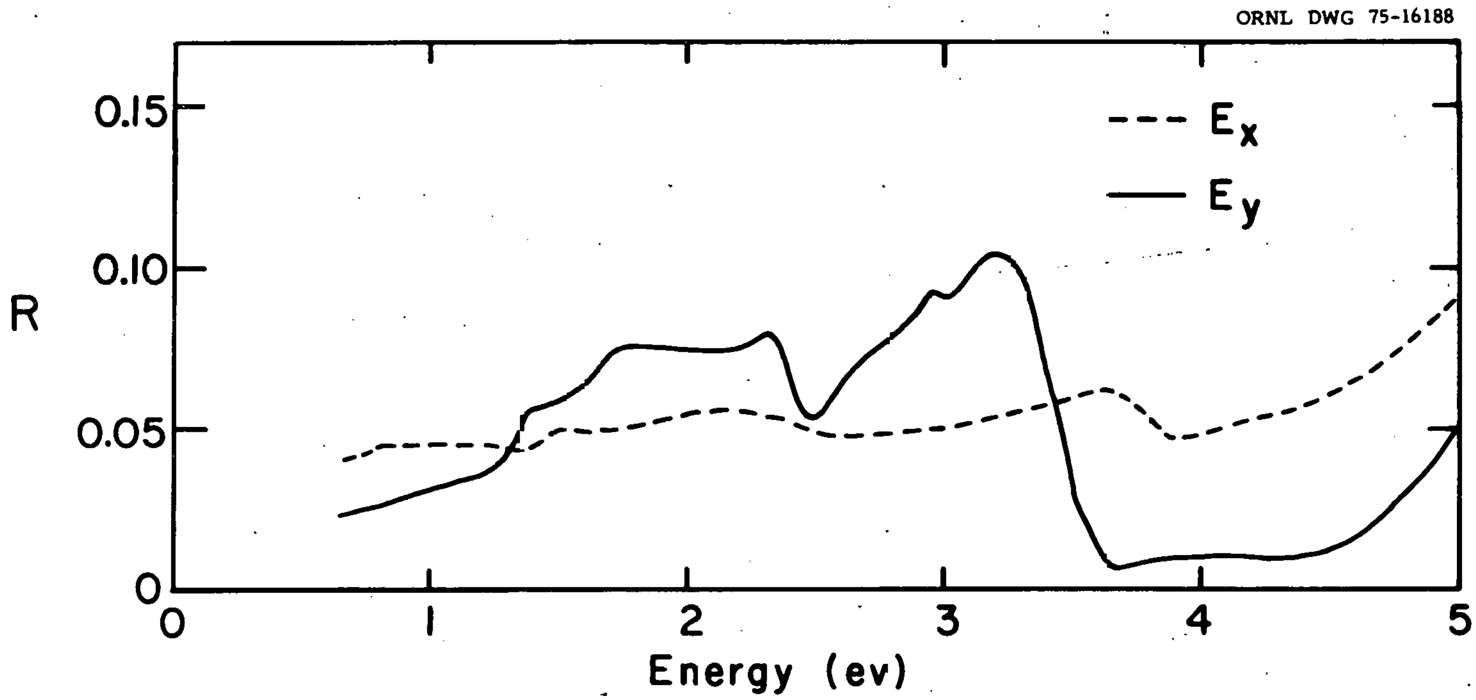

Figure 12. Reflectance of Orthorhombic TTF-I_r.

The parameters were then varied to obtain the best fit to the reflectance data (see Appendix II). This fitting procedure insures the proper relationships between the dielectric functions ϵ_1 and ϵ_2. The fitted reflectance curves were very close to the experimental curves, especially above 2 eV.

The optical properties determined by the above procedure are shown in Figures 13 and 14. The optical conductivity $\sigma(\omega) = \epsilon_2 \omega/4\pi$ (oscillator strength density) is plotted rather than ϵ_2 since it corresponds more closely to the solution absorption spectra. The oscillator parameters are given in Table I.

Figure 14 the vertical lines indicate the positions[32] of the solution absorption peaks for TTF^+. The oscillator strengths (proportional to the heights of the lines) and polarizations were determined by a Pariser-Parr-Pople molecular orbital calculation.[33] Note that the major structure for orthorhombic $TTF\text{-}I_n$ corresponds very well in energy, relative strength, and polarization. Also, the dominant structure is the same for monoclinic $TTF\text{-}I_n$ (see also Figs. 10 and 12).

The TTF^+ spectrum seems to account for all the major structure except for the peak around 4 eV in both the monoclinic spectrum and the y-axis polarized orthorhombic spectrum. There are three peaks in the solution absorption of the I_3^- ion occurring

ORNL DWG 75-16189

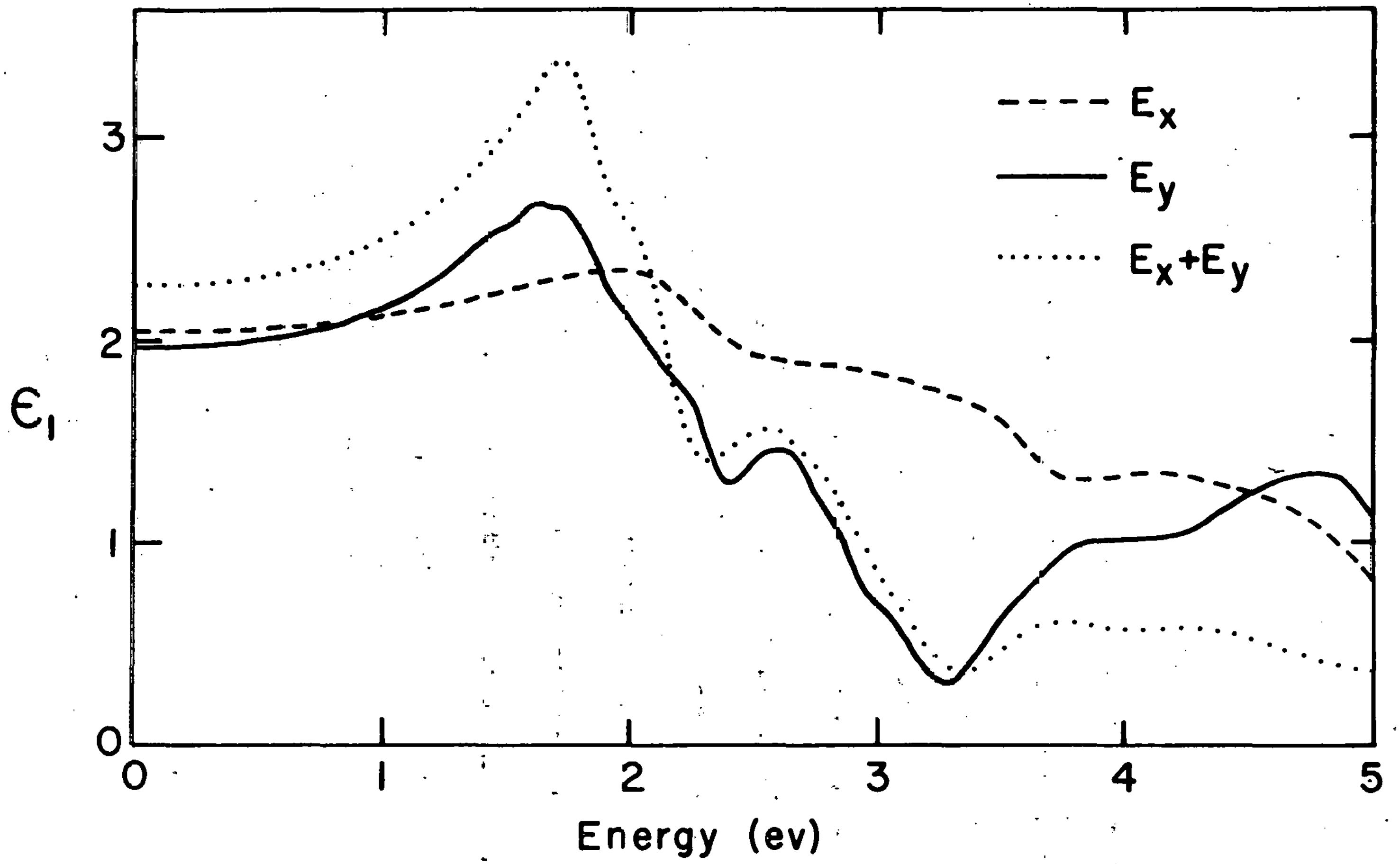

Figure 13. $\epsilon_1(\omega)$ for the TTF-I_n Crystals.

Dotted curve: monoclinic TTF-I_n perpendicular to the stacking axis. Solid and dashed curves: orthorhombic TTF-I_n

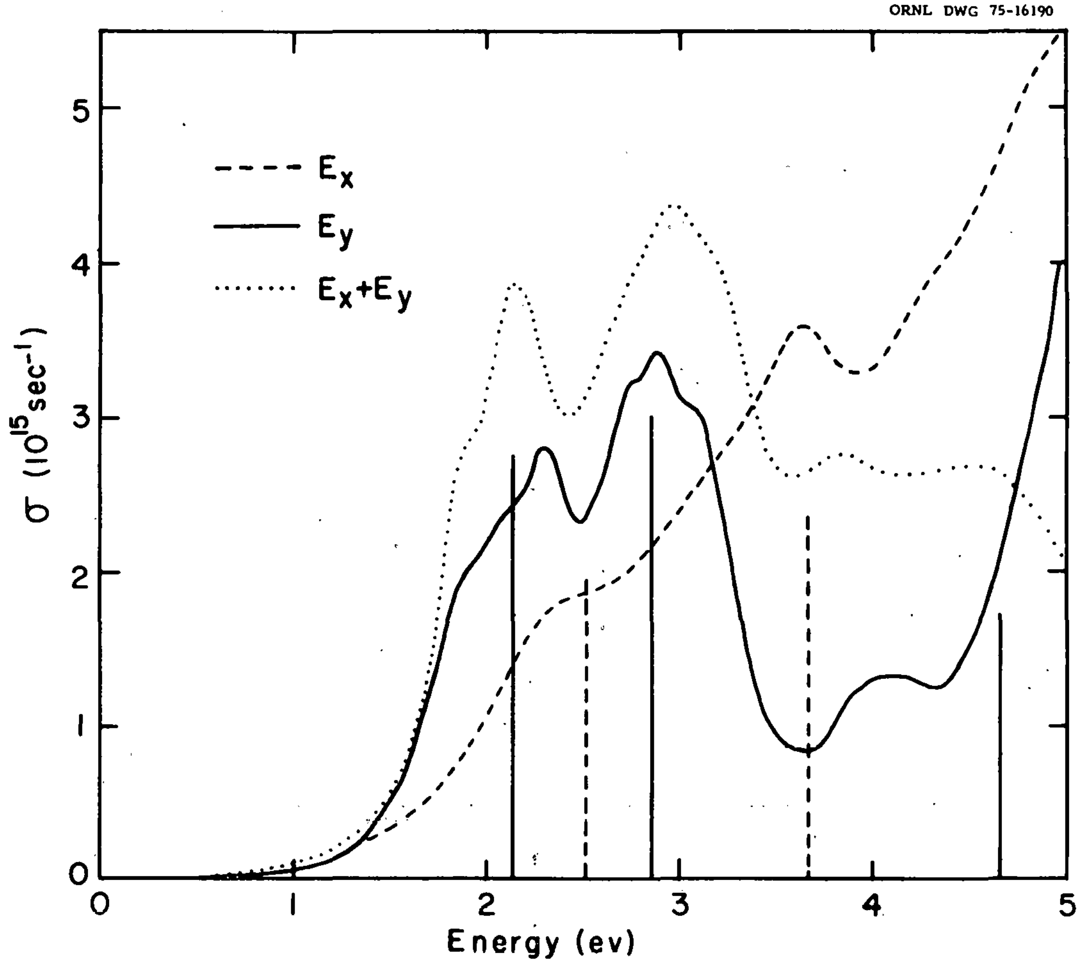

Figure 14. $\sigma(\omega)$ for the TTF-I_n Crystals.

Dotted curve: monoclinic TTF-I_n perpendicular to the stacking axis. Solid and dashed curves: orthorhombic TTF-I_n. Vertical lines indicate the positions of solution absorption peaks for TTF^+ and their calculated polarizations.

TABLE I

Lorentzian Oscillator Parameters

$\epsilon_{core} = 1$

	Oscillator #	$\hbar\omega_i$	$\frac{4\pi\hbar^2 Ne^2}{m} f_i$	$\hbar\Gamma_i$
Orthorhombic TTF-I_n Y-polarized	1	1.86 eV	0.55 eV	0.3 eV
	2	2.16	1.64	.45
	3	2.72	1.9	.7
	4	2.98	.9	.45
	5	3.23	.86	.45
	6	3.80	1.5	2.0
	7	3.85	.75	.65
	8	4.28	.2	.65
	9	4.7	3.05	1.3
Orthorhombic TTF-I_n X-polarized	1	2.33	1.2	.9
	2	3.33	3.8	1.6
	3	3.64	.54	.47
	4	4.26	.5	.65
	5	5.1	10.4	1.61
Monoclinic TTF-I_n	1	1.5	.03	.2
	2	1.67	.03	.14
	3	1.86	.56	.37
	4	2.10	.62	.4
	5	2.68	.95	.5
	6	2.73	.03	.1
	7	2.32	.55	.3
	8	2.91	.93	.38
	9	3.12	.39	.26
	10	3.25	.2	.23
	11	3.89	.12	.25
	12	4.03	.08	.2
	13	4.18	.11	.25
	14	5.15	5.2	.86

at 2.85 eV, 3.50 eV, and 4.25 eV.[34] Though the latter two peaks are strong (molar extinction coefficients of 26,000 and 39,000, respectively), they are polarized along the axis of the molecule (which is along the stacking axis in orthorhombic TTF-I_n) and thus would be reduced an order of magnitude in the orthorhombic TTF-I_n spectrum here. The latter I_3^- solution peak must be shifted ~0.3 eV to account for the peak at 4.0 eV in the solid state spectrum. This shift in energy might plausibly account for the 4 eV peak in orthorhombic TTF-I_n but cannot account for the peak in the monoclinic spectrum since no I_3^- species is found in the x-ray data.

The solution spectrum of neutral TTF shows two absorption peaks at 4.0 eV (strong) and 3.4 eV (weak) which are polarized along the x and y axes respectively of the TTF molecule.[35] Thus the weak peak at 4 eV in the solid state spectra might be due to the presence of a small amount of neutral TTF in both monoclinic and orthorhombic crystal structures. This, of course, assumes the charges within each TTF stack to be localized for the time scale of molecular electronic transitions.

From results of x-ray data, a partial charge transfer from the TTF stacks to the iodine columns is expected. The ionization potential of TTF is low (6.95 eV)[36] while the electron affinity of iodine is high (2.8 eV).[37] Thus in monoclinic TTF-I_n, where only iodine monomers are found, the charge transfer should be given by the stoichiometry, i.e., ~ 0.7 electrons are transferred per TTF molecule. Thus, the 4 eV peak in the solid state spectrum of monoclinic TTF-I_n seems to be fully accounted for by the presence of a small amount of neutral TTF.

The charge transfer in orthorhombic TTF-I_n is less well-defined from x-ray structure, since the exact population of each polyiodide species is unknown.[27] Each monomer and trimer should be singly charged. If dimers are present, they are probably neutral or negatively charged. The internuclear lengths for I_2^o and I_2^- are 2.666 Å[38] and ~ 3.5 Å (estimated)[39] respectively, neither of which correspond very closely to the A-site to A-site distance of ~ 3 Å. The electronic affinity of I_2 is 2.5 eV[40] indicating that the dimer might be charged. A charge transfer of 1.0e per TTF molecule is given by both the pure trimer-monomer (TM) species and the TMTMD species (in closer agreement with structural information), assuming all polyiodide species to be singly charged. If the dimers are uncharged, however, the charge transfer for the TMTMD species is 0.8e per TTF.

An effect which favors a lower value of charge transfer is the fact that electrostatic repulsion within the TTF stacks increases with the amount of charge transfer. The 1:1 TTF-Br crystal structure contains stacks of alternating TTF dimers and bromine dimers,[29] indicating that fully charged segregated stacks of TTF and Br may be unstable.

If the peak at 4 eV in orthorhombic TTF-I_n is assumed to be primarily due to the presence of neutral TTF molecules, then a crude calculation of the charge transfer can be made by comparing the peak at 2.86 eV due to TTF^+ to the 4 eV peak. Using a minimum number of oscillators to fit the y-axis polarized reflectance, the ratio of the oscillator strengths for the TTF^+ and TTF^o peaks, using the expression

$$\frac{C_{TTF^o}\,\epsilon_{TTF^o}}{C_{TTF^+}\,\epsilon_{TTF^+}} = \frac{f_{TTF^o}}{f_{TTF^+}} \qquad (16)$$

where C is the concentration, ϵ is the solution extinction coefficient, and f is the fitted oscillator strength, gives the percentage of charged TTF molecules as ~ 80%. This result is in agreement with the charge transfer calculated from the crystal structure containing repeated units of TMTMD polyiodide species with uncharged dimers.

Thus structural and optical information indicate a charge transfer of ~ 0.7e per TTF in monoclinic TTF-I_n and ~ 0.8 - 1.0e per TTF in orthorhombic TTF-I_n. Although experimental data tends to favor the lower value of charge transfer in orthorhombic TTF-I_n, a fully charged structure cannot be absolutely ruled out.

An important feature of the optical study is that it provides the first experimental determination of the polarizations of the electronic transitions of TTF^+ occurring in the visible region of the spectrum. Solution measurements cannot yield any polarization data since the molecules are randomly aligned. Meaningful polarization measurements on TTF within the TTF-TCNQ crystal structure are difficult because the TTF molecules are titled with respect to the stacking axis by ± 24.5°.[41] Polarized absorption studies have been made on neutral TTF using the stretched film technique.[35]

Conductivity

Figure 15 shows the measured conductivity of a typical sample of TTF-TCNQ. For the five samples measured, the room temperature conductivity was between 413 $(\Omega\text{-cm})^{-1}$ and 432 $(\Omega\text{-cm})^{-1}$ while the ratio of peak conductivity (near 58°K) to the room temperature value was between 8 and 23. These values are typical of the results of the majority of workers in this field[6] and present no indication of the anomalously high values reported for a few samples by one group of workers.[7]

Shown in Figure 16 is the conductivity along the other two axes of TTF-TCNQ. The dashed line indicates no data was taken in this area. The a axis conductivity was measured using the Montgomery configuration[25] and by painting current electrodes along the edges of

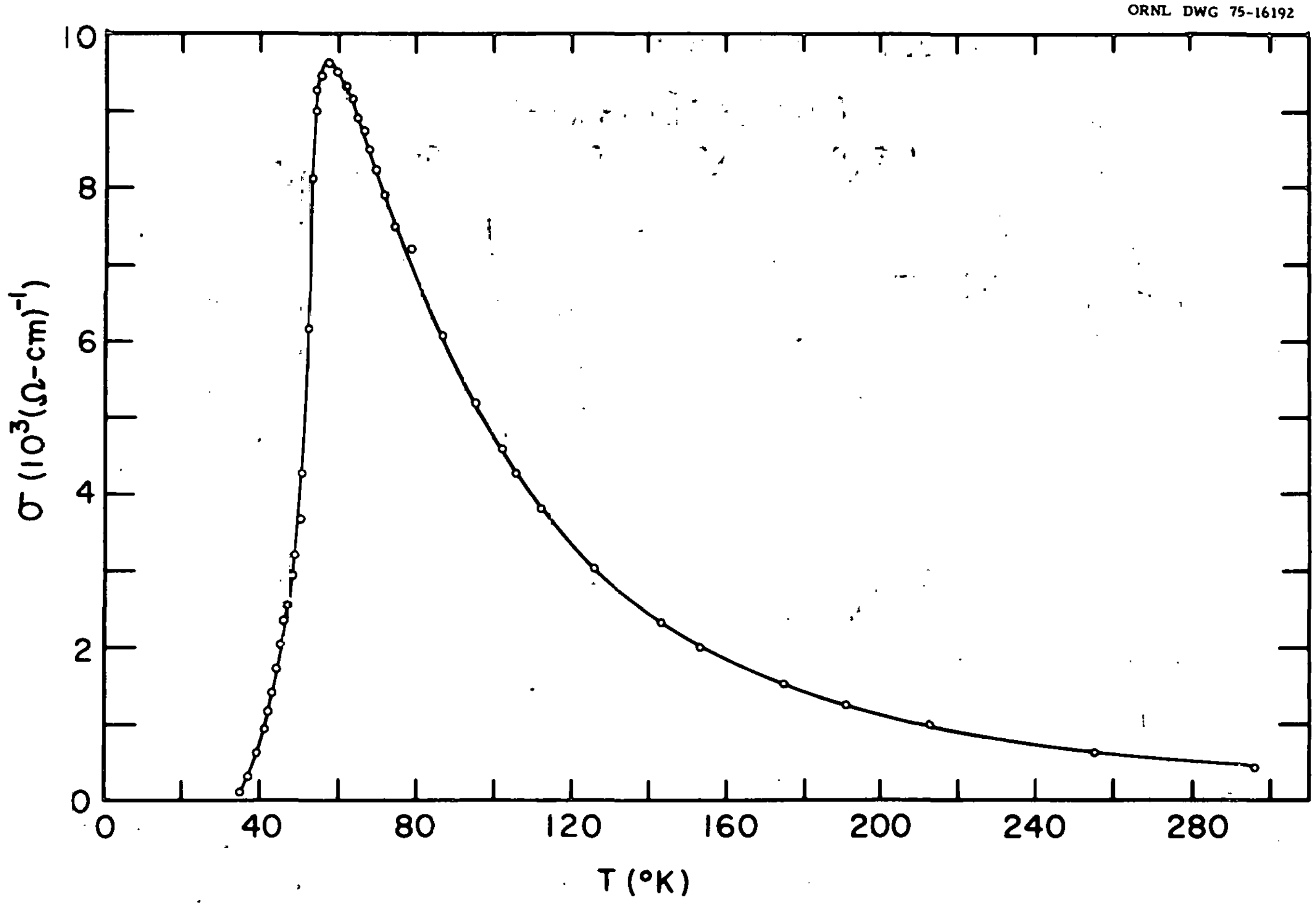

Figure 15. Longitudinal Conductivity of TTF-TCNQ.

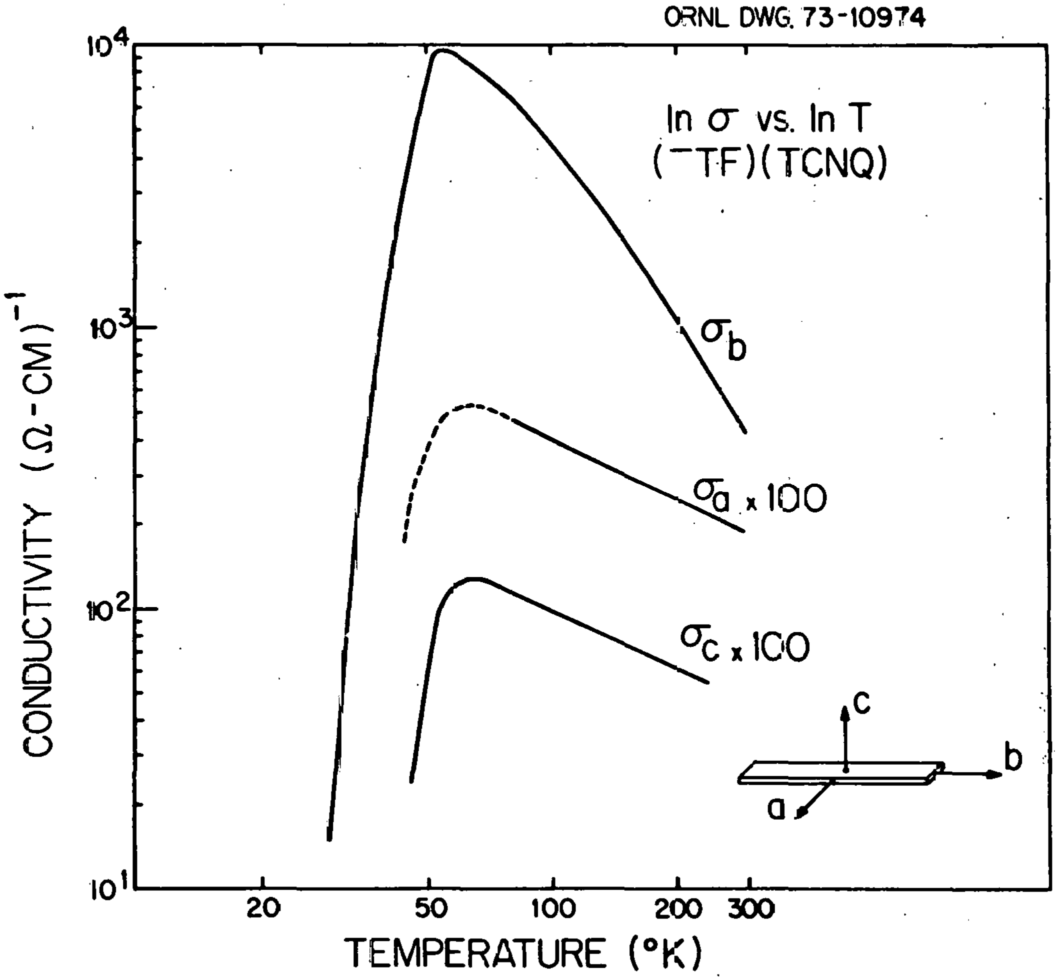

Figure 16. Anisotropic Conductivity of TTF-TCNQ.

the sample. The c^* axis conductivity was measured by painting current electrodes over the two faces of the crystal. Difficulties in finding perfect crystal specimens, making good, uniform contacts, and measuring the dimensions of the crystals limit the absolute accuracies of these curves, but the extreme anisotropy is clearly demonstrated.

The conductivities along the stacking axis of various forms of the TTF-halides are shown in Figures 17 through 20. Figure 20 compares typical results obtained in the conductivity measurements on all forms of charge transfer salts in this thesis. Room temperature values, activation energies (ΔE in Equation 1), and approximate transition temperatures are collected in Table II.

The conductivity of monoclinic TTF-Br_n (Figures 17 and 18) showed almost no temperature dependence for a wide thermal range near room temperature. Above 320°K a very slight decrease in conductance could be reproducibly seen. Below 180°K the conductance fell into an exponential region typical of thermal activation of electrons across a constant energy gap. Temperature cycling produced no observable changes in the conductivity curves.

The differences in room temperature conductivities and activation energies of the two samples of TTF-Br_n measured (shown in Figure 17) must have been due to the samples themselves. Although contact resistances were typically an order of magnitude larger than the

ORNL DWG 75-16182

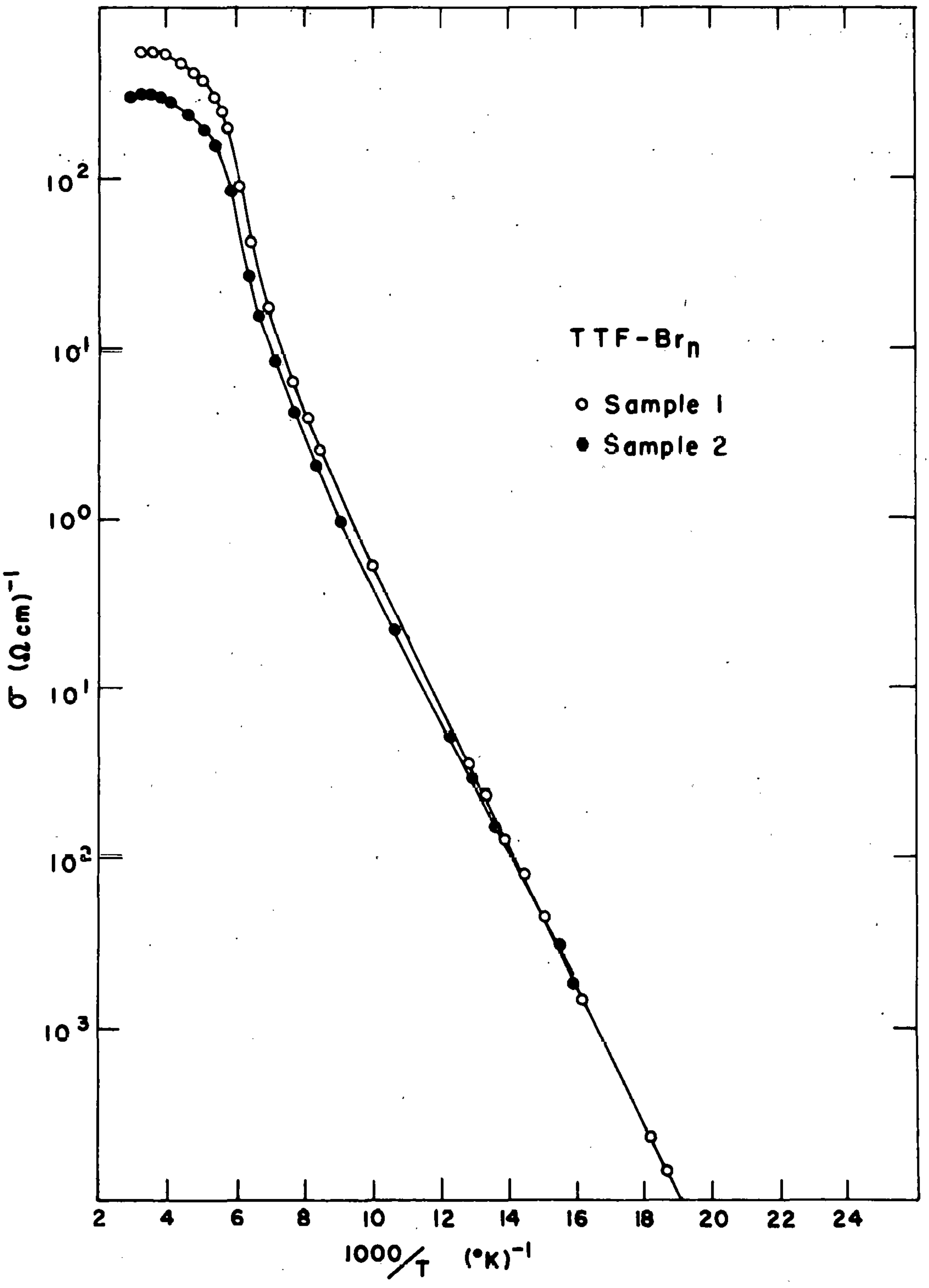

Figure 17. Conductivity of Monoclinic TTF-Br$_n$.

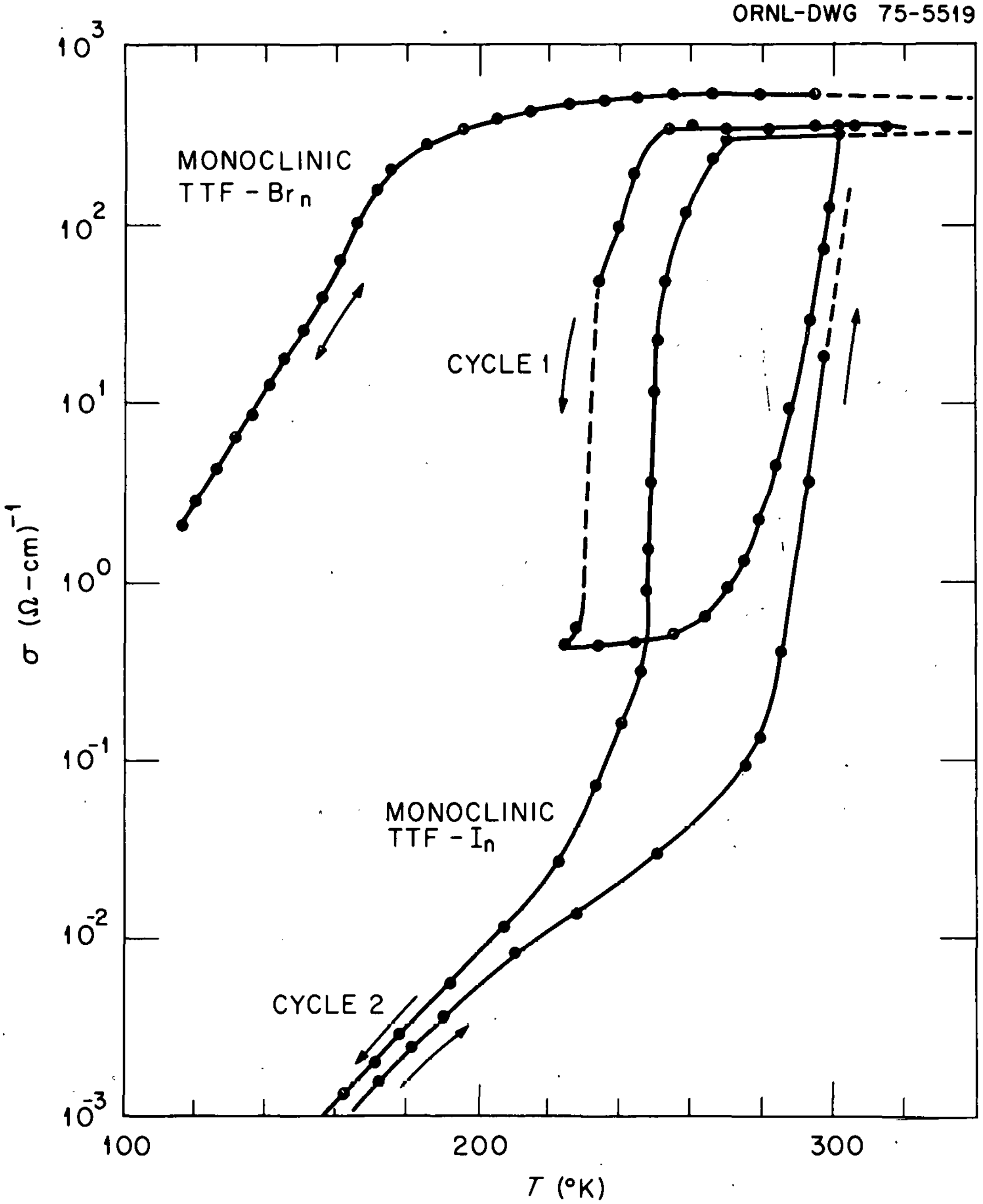

Figure 18. Conductivity of Monoclinic TTF-I_n.

ORNL DWG 75-16186

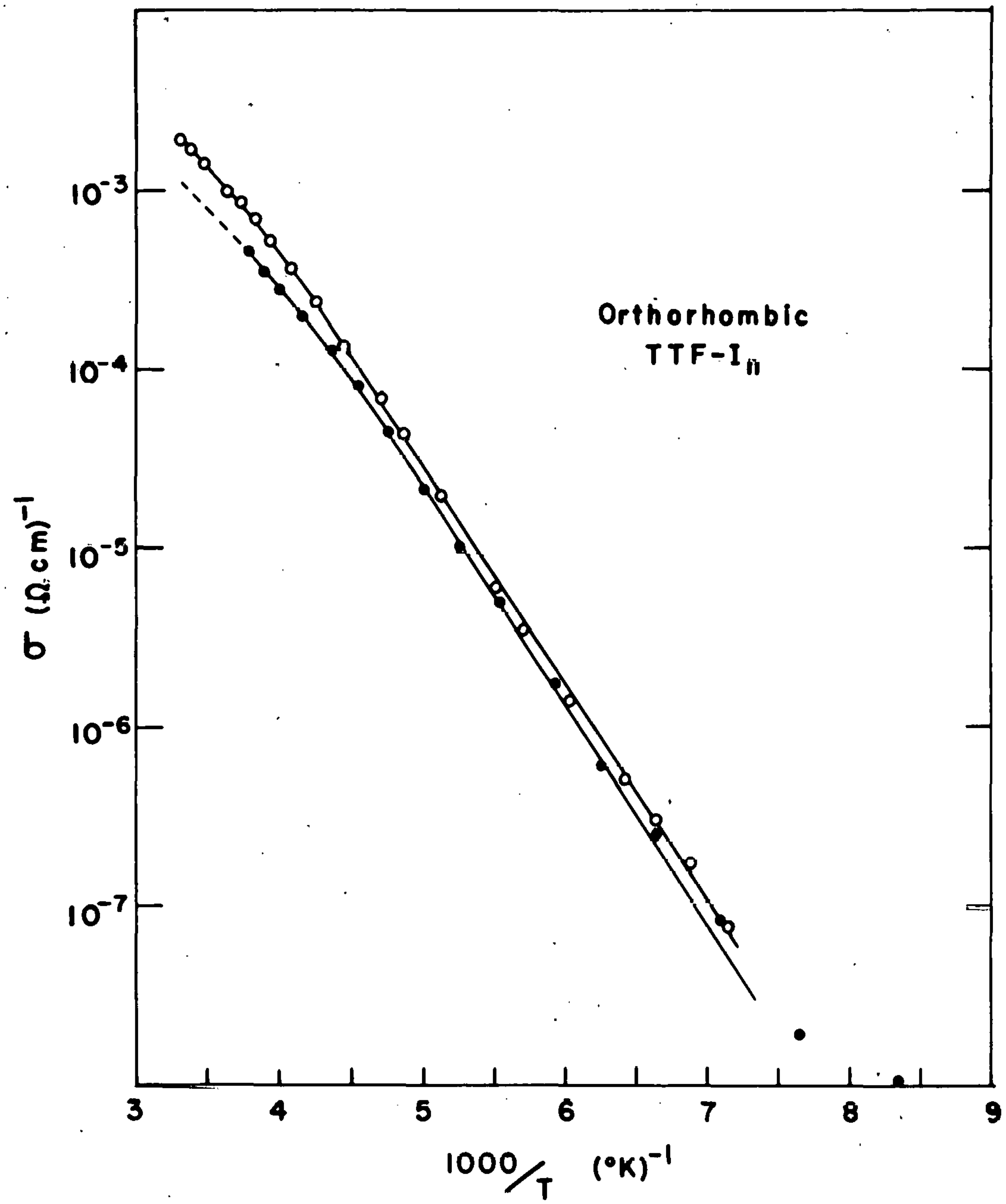

Figure 19. Conductivity of Orthorhombic TTF-I_n.

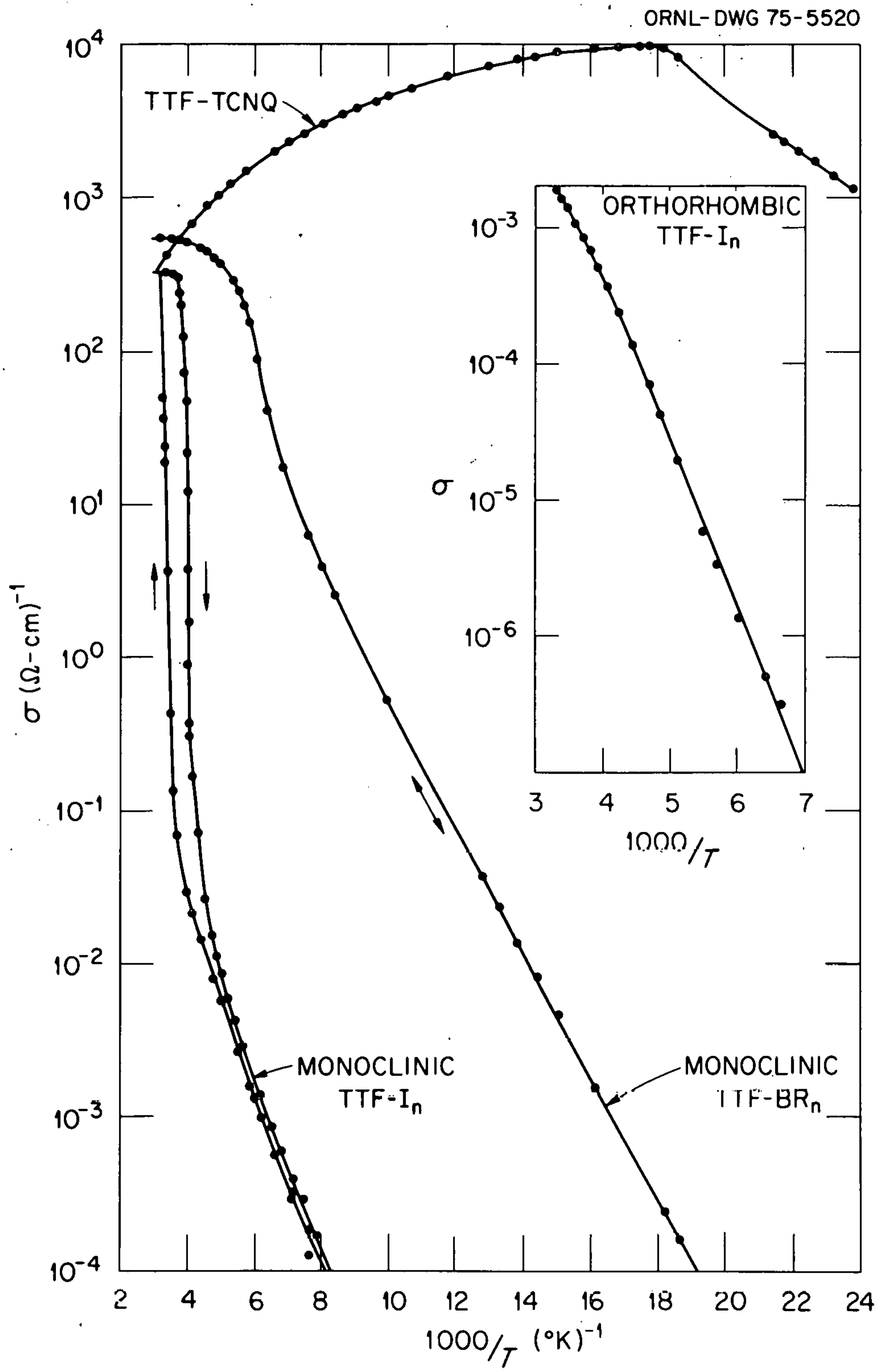

Figure 20. Conductivities of Charge Transfer Salts Compared.

TABLE II

Electrical Characteristics of the TTF-Halides

	Sample	Cycle	$\sigma(\Omega\ \mathrm{cm})^{-1}$ @ 300°K	Transition Temperature (°K)	ΔE(eV)
Monoclinic $TTF\text{-}Br_n$	1	1,2	500	180	0.0808
	2	1	310	180	0.0785
Monoclinic $TTF\text{-}I_n$	1	1	344	250	-*
	1	2	348	260	-
	1	3	333	270	-
	2	1	302	260	-
	3	1	133	220	-
	3	2	-	235	-
	4	1	100	205	-
	5	1	216	225	-
	6	1	428	225	-
Orthorhombic $TTF\text{-}I_n$	1	1	1.9×10^{-3}	-	0.241
	2	1	1×10^{-3}	-	0.243
	3†	1	5.8×10^{-3} ††	-	0.259
	4†	1	2.6×10^{-3} ††	-	0.216

---

*The activation energy for monoclinic $TTF\text{-}I_n$ varied from ~ 0.12 eV just below the transition temperature to 0.084 eV at lower temperatures.

†Two-probe conductivity sample

††Straight line extrapolation to 300°K

sample resistance, checks revealed no inhomogeneous current distributions. Inaccuracies in measuring physical dimensions (estimated error within 30%) would only shift the entire curve vertically when plotted on log paper. The observed differences, therefore, may have been due to unknown factors such as breaks in the conduction paths, impurities, or different stoichiometries.

The isostructural iodine compound, monoclinic TTF-I_n, showed a similar behavior—a broad, almost flat conductance near room temperature and a fall into an exponential region at low temperatures (Figure 18). Several striking differences were observed, however.

The transition from the flat region into the exponential region occurred at different temperatures for various samples and was not constant for repeated temperature cyclings of the same sample. This probably indicates not only that there were differences between the samples but that changes within each sample took place in temperature cycling. The transition was therefore affected by an uncontrolled parameter such as thermal stress. Apparently, considerable mechanical stress was exerted upon the samples since two samples fractured during the cooling cycle.

Another effect was noticed in some samples. Upon cooling the samples through the transition region a very sharp decrease in conductivity was occasionally detected, followed by the characteristic exponential behavior. This decrease proceeded with time even if the temperature was held constant (to within ± 0.2°K). Though no thermal stress was received by the sample, some changes within the sample took place, possibly local shifts in the equilibrium positions of the molecules which would not necessarily happen simultaneously if the sample were not perfectly homogeneous.

The most dramatic effect observed was a large hysteresis between the heating and cooling curves. This phenomenon was seen at any point in the temperature cycle but was most pronounced near the transition region. The original room temperature conductance of each sample was restored by warming the sample to a point between 260°K and 320°K depending upon the sample. The fact that hysteresis was seen in every sample indicates that a phase transformation with supercooling and superheating took place. Preliminary x-ray results of TTF-I_n at low temperature reveal no major change in crystal structure,[27] but very significant changes in conductivity are possible with only minor changes in x-ray structure.[42]

It is remarkable that the isostructural TTF-Br_n showed absolutely no hysteresis. Assuming a similar charge transfer in both complexes (i.e., each halogen having a charge of -e), the observed differences are difficult to explain. The dimensions of the unit cell in the bromine complex are slightly smaller than that in the iodine complex,[43] but this difference can be attributed to the size of the halogen ions. A possible explanation may be that a slight change in unit cell dimensions provides another equilibrium position of the iodine ions which is metastable at low temperatures. This might cause the TTF molecules to dimerize to some extent which results in the lower conductivity.

Orthorhombic TTF-I_n exhibited a qualitatively different conductivity behavior along the stacking axis (Figure 19). The conductivity was thermally activated over the entire temperature range, following a straight line when plotted as $\ell n \sigma$ vs T^{-1} except for a slight deviation above 250°K (see Figure 19). The two four-probe curves plotted are almost identical if shifted vertically to allow for error in the measurement of physical dimensions. Two samples were also constructed with voltage electrodes directly across the thin dimension of the samples, and the opposing voltage due to the proximity of the current electrodes was found to be at least four orders of magnitude less than that observed in the four-probe arrangement of Figure 5 (see page 22). This was due to the fact that the conductivity (as measured by the Montgomery method) along the axes perpendicular to the stacking axis was about 2×10^{-5} $(\Omega\text{-cm})^{-1}$ to 3×10^{-5} $(\Omega\text{-cm})^{-1}$ at room temperature or about two orders of magnitude lower than that along the stacking axis. With correction for contact resistance, two-probe measurements on these crystals agreed well with four-probe results.

In all forms of the TTF-halides reported here, conduction is believed to occur along the TTF stacks because of the large overlap between adjacent molecules within each stack. In the iodine columns the overlap is very small since the distance between adjacent iodine ions is about 5 Å in the monoclinic form and either 4 Å or 5 Å for the spacing between small polyiodide units in the orthorhombic form. Thus, if a charge transfer has partially emptied the uppermost band of the TTF stacks then conduction is possible.

On the other hand, small distortions within the TTF stacks or disorder introduced by the iodine columns can upset the conduction mechanism. Apparently the distortions in monoclinic TTF-I_n and TTF-Br_n are insufficient to prevent these crystals from being good organic conductors at room temperature. Qualitatively, we can see that small rotations of the TTF molecules about the stacking axis would probably not upset the molecular orbital overlap as much as small rotations perpendicular to the stacking axis. This may be a primary factor in the difference in the conductivities between the orthorhombic and monoclinic crystals.

The amount of charge transfer can also play a role in the conduction process, particularly if there is a complicated band structure. For example, if a distortion such as a dimerization were to split the conduction band in half then conduction could only be thermally activated when the charge transfer is one electron per molecule. However, for other fractional amounts of charge transfer, a band would be left partially filled and thus conducting.

If a band picture is applicable to the orthorhombic TTF-I_n structure then a semiconducting behavior would be expected if the conduction band were split in half and the charge transfer were exactly one electron per TTF molecule. The optical and structural data tends to favor less than a full electron transfer so that the conductivity behavior may be viewed as a hopping conduction in which electrons must be thermally activated across spatial energy gaps.

Another difference between the monoclinic and orthorhombic structures which may affect the conduction process is that in the monoclinic structure alternate stacks of TTF molecules are rotated 90°. Thus each stack of TTF molecules is presented on two sides by adjacent TTF stacks which have their high polarizable axes directed toward that stack. This might help to reduce the electron-electron coulomb repulsion (via electron screening) for electrons within each TTF stack. A similar situation is seen in NMP-TCNQ where the NMP stacks act as highly polarizable side chains.

CHAPTER V

SUMMARY

The results of our work on TTF-TCNQ produced no new results but confirmed the results that were concurrently obtained by other laboratories.[6] In particular, no unusually high conductivities observed for a very few samples in one laboratory[7] were seen.

The conductivities for the TTF-halides presented unusual behaviors. The monoclinic crystals had a high conductivity at room temperature, as good as some of the best organic conductors. While monoclinic TTF-I_n had a large hysteresis between heating and cooling curves, monoclinic TTF-Br_n exhibited a similar behavior but with absolutely no measurable hysteresis. These results have since been confirmed by other laboratories.[44,45] Conduction in these crystals is believed to occur along the stacks of TTF molecules where rotational distortion along the stacking axes does not apparently upset this process. Orthorhombic TTF-I_n had a much lower conductivity at room temperature, being thermally activated over the entire temperature range studied. The difference between the conductivities of the monoclinic and orthorhombic crystals is probably due to rotational distortion perpendicular to the stacking axes in orthorhombic TTF-I_n, which can upset the molecular overlap sufficiently to create spacial gaps across which electrons must be thermally activated. Another possible explanation may be that the charge transfer in the orthorhombic crystals occurs at a band splitting.

The optical reflectance data indicated that a low energy electron transfer occurred for light polarized along the stacking axes of monoclinic TTF-I_n. The reflectance of the orthorhombic crystal gave the first polarization data for the in-plane electronic transitions of the TTF^+ molecules. The reflectances involving the in-plane transitions of the TTF molecules were similar in both crystal forms. The charge transfer calculated from x-ray data on monoclinic TTF-I_n was confirmed by the presence of a weak peak in its optical spectrum corresponding to a small amount of neutral TTF molecules. A similar peak was observed in orthorhombic TTF-I_n which may indicate the presence of some neutral TTF, but the possibility of a full electron transfer could not be absolutely ruled out.

PAGES 66 to 68

WERE INTENTIONALLY

LEFT BLANK

BIBLIOGRAPHY

1. Shchegolev, I. F., Phys. Stat. Sol. (a) 12, 9 (1972).
2. Soos, Z. G., Ann. Rev. Phys. Chem., 121 (1974).
3. Cohen, M. J., Coleman, L. B., Garito, A. F., Heeger, A. J., Phys. Rev. B 10, 1298 (1974).
4. Warmack, R. J., Callcott, T. A., Schweinler, H. C., Appl. Phys. Lett. 24, 635 (1974).
5. Bright, A. A., Garito, A. F., and Heeger, A. J., Phys. Rev. B 10, 1328 (1974).
6. Thomas, G. A., et al., preprint, submitted to Phys. Rev. B.
7. Coleman, L. B., Cohen, M. J., Sandman, D. J., Yamagishi, F. G., Garito, A. F., and Heeger, A. J., Solid State Commun. 13, 943 (1973).
8. Schafer, D. E., Wudl, F., and Thomas, G. A., Solid State Commun. 14, 347 (1974).
9. Bickford, L. R. and Kanazawa, K. K., preprint, submitted to J. Phys. Chem. Solids.
10. Heeger, A. J. and Garito, A. F., preprint (1975).
11. Ferraris, J. P., Cowan, D. O., Walatka, Jr., V. V., and Perlstein, J. H., J. Am. Chem. Soc. 95, 948 (1973).
12. Peierls, R. E., "Quantum Theory of Solids", (Oxford, London, 1955) p. 108.
13. Comes, R., Denoyer, F., Garito, A. F. and Heeger, A. J., preprint submitted to Phys. Rev. Lett.
14. Mook, H., private communication.

15. Grobmann, W. D., Pollak, R. A., Eastman, D. E., Maas, Jr., E. T. and Scott, B. A., Phys. Rev. Lett. 32, 534 (1974).

16. See for example, Lee, J. D., "Concise Inorganic Chemistry" (Van Nostrand, London, 1964).

17. See for example, Seitz, F., "The Modern Theory of Solids" (McGraw-Hill, New York, 1940).

18. Kistenmacher, T. J., Pyle, R. E., Banks, R. and Phillips, T. E., Bull. Am. Phys. Soc. 20, 466 (1975).

19. Epstein, A. J., Etemad, S., Garito, A. F. and Heeger, A. J., Phys. Rev. B5, 952 (1972).

20. See for example, Wooten, F., "Optical Properties of Solids" (Academic Press, New York, 1972).

21. Hertzberg, G., "Molecular Spectra and Molecular Structure," Vol. III (Nostrand, Princeton, 1966).

22. Löwdin, P. and Pullman, B., editors "Molecular Orbitals in Chemistry, Physics, and Biology" (Academic, New York, 1964).

23. Compton, R. N., private communication.

24. Blankenship, Jr., J. L., PhD thesis (University ot Tennessee, 1973) (unpublished).

25. Montgomery, H. C., J. Appl. Phys. 42, 2971 (1971).

26. Lambrecht, Karl, Crystal Optics Co. Glan prism.

27. Johnson, C. K., Watson, C. R., and Warmack, R. J., Amer. Cryst. Assoc. Meeting Program and Abstracts 3, 19 (March 1975); Johnson, C. K. and Watson, C. R., to be published; Johnson, C. K., private communication.

28. Wiebenga, E. H. and Kracht, D., Inor. Chem. 8, 738 (1969).

29. Scott, B. A., Torrance, J. B., LaPlaca, S. J., Cornfield, P. Green, D. C., and Etemad, S., Bull. Am. Phys. Soc. 20, 496 (1975).

30. Gutman, V., editor, "Halogen Chemistry" (Academic, London, 1967), p. 284.

31. Grant, P. M., Greene, R. L., Wrighton, G. C. and Castro, C., Phys. Rev. Lett. 31, 1311 (1973).

32. Hunig, S., Kiesslich, G., Quast, H. and Scheutzow, D., Liebigs Ann. Chem. 310 (1973).

33. Zahradnik, R., Carsky, P., Hunig, S., Kiesslich, G., and Scheutzow, D., Int. J. Sulfur Chem. C6, 109 (1971).

34. Gabes, W., and Nijman-Meester, M. A. M., Inor. Chem. 12, 589 (1973).

35. Gleiter, R., Schmidt, E., Cowan, D. O., and Ferraris, J. P., J. Electron Spectroscopy and Related Phenomena 2, 207 (1973).

36. Klots, C. E., Compton, R. N., and Raaen, V. F., J. Chem. Phys. 60, 1177 (1974).

37. Ref. 30, p. 5.

38. Mulliken, R. S., J. Chem. Phys. 55, 288 (1971).

39. Mulliken, R. S., J. Am. Chem. Soc. 72, 600 (1950).

40. Tang, S. Y., Leffert, C. G., and Rothe, E. W., J. Chem. Phys. 62, 132 (1975).

41. Kistenmacher, T. J., Phillips, T. E., and Cowan, D. O., Acta Cryst. B30, 763 (1974).

42. Blessing, R. H., and Coppens, P., Solid State Commun. 15, 215 (1974).

43. La Placa, S. J., Weidenbosner, J. E., Scott, B. A., and Cornfield, P., Bull. Am. Phys. Soc. 20, 496 (1975).

44. Johnson, G. R., Dahm, D. J., Miles, M. G., and Wilson, J. D., Bull. Am. Phys. Soc. 20, 466 (1975); Scott, B. A., private communication.

45. Somoano, R. B., Gupta, A., Hadek, V., Datta, T., Jones, M., Deck, R., and Hermann, A. M., preprint, submitted to J. Chem. Phys.

APPENDIXES

PAGES 73 to 74

WERE INTENTIONALLY

LEFT BLANK

APPENDIX I

Calculation of Apparent Conductivity

The positions of the electrical contacts in conductivity measurements can be very critical, especially in the case of highly anisotropic conductors. Most of the longitudinal conductivities reported for TTF-TCNQ use the conventional four-probe technique in which four parallel wires coated with silver paint make contact across the wide face of the sample. This method requires uniform current flow in the sample between the voltage probes. If the actual contacts produced were only small areas rather than contacts across the entire width of the face, then a nonuniform current distribution would be set up resulting in an anomalous apparent conductivity. The results of a model calculation for the apparent conductivity are detailed in the following.

Consider an array of parallel line charges in free space, with alternating line charge densities of $+\lambda$ and $-\lambda$. If the charges are located on the real axis (x) of the complex plane then the potential at any point $z = x + iy$ is

$$V = \frac{-\lambda}{2\pi\epsilon_o} R_e \left\{ \sum_{n=-\infty}^{\infty} (-1)^n \ln\left(\frac{Z + nL}{n_o}\right) \right\}$$

where ϵ_o is the permittivity of free space, L is the spacing between line charges, and r_o fixes the reference potential. The summation converges very slowly, even with the aid of a computer. It was transformed into a much more rapidly converging series by H. C. Schweinler of Oak Ridge National Laboratory:

$$\text{Re} \sum_{n=-\infty} (-1)^n \ln\left(\frac{Z+nL}{r_o}\right) = \text{Re} \ln\left\{\frac{Z}{Z-L} \cdot \frac{Z-2L}{Z+L} \cdot \frac{Z+2L}{Z-3L} \cdots\right\}$$

$$= \text{Re} \ln\left\{\frac{\left[\left(\frac{Z}{L}\right)\frac{2^2}{3^2} \cdot \frac{4^2}{5^2} \cdots\right]\left(1-\frac{(Z/L)^2}{2^2}\right)\left(1-\frac{(Z/L)^2}{4^2}\right)\cdots}{\left(1-\frac{Z^2}{L^2}\right)\left(1-\frac{(Z/L)^2}{3^2}\right)\left(1-\frac{(Z/L)^2}{5^2}\right)\cdots}\right\}$$

$$= \text{Re} \ln\left\{\frac{\sin(Z\pi/2L)}{\cos(Z\pi/2L)}\right\}$$

$$= \frac{1}{2} \ln\left\{\frac{\sin^2\left(\frac{\pi x}{2L}\right) + \sinh^2\left(\frac{\pi y}{2L}\right)}{\cos^2\left(\frac{\pi x}{2L}\right) + \sinh^2\left(\frac{\pi y}{2L}\right)}\right\}$$

If the parallel sets of alternating line charges are also positioned along the y axis (see Fig. 21), then the potential is, by superposition:

$$V = \frac{-\lambda}{4\pi\epsilon_o} \sum_{n=-\infty}^{\infty} \ln\left\{\frac{\sin^2\left(\frac{\pi x}{2L}\right) + \sinh^2\left[\frac{\pi(y-2nW)}{2L}\right]}{\cos^2\left(\frac{\pi}{2L}\right) + \sinh^2\left[\frac{\pi(y-2nW)}{2L}\right]}\right\}$$

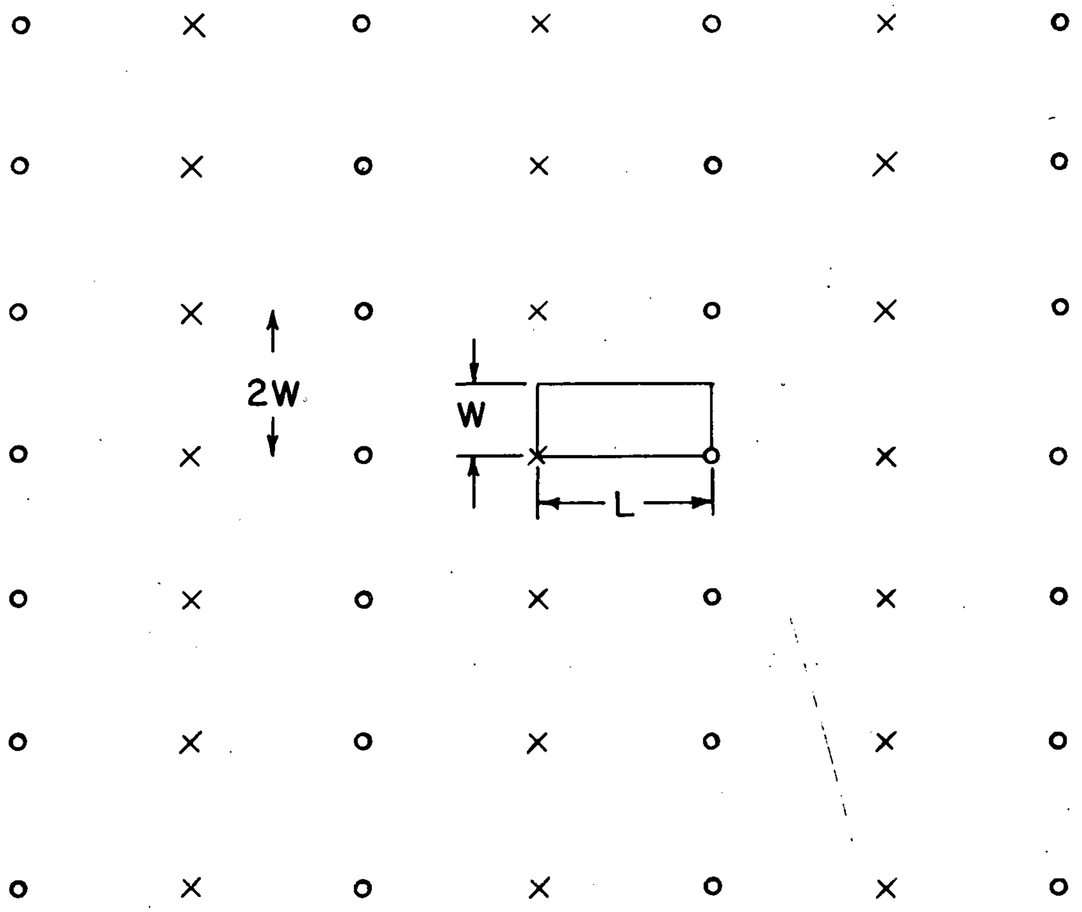

Figure 21. Method of Image Applied to the Apparent Conductivity Problem.

Circles and crosses indicate the positions of positive and negative line charges, or current sources and sinks.

By considering the method of images, we can apply this result to the problem of a conducting rectangular parallelopiped of thickness t with current electrodes located on two corners (see Fig. 21). The line charges are then considered to be current sources and sinks, and the replacement is made:

$$\frac{\lambda}{\epsilon_o} \rightarrow \frac{4I}{\sigma_m t}$$

where σ_m is the conductivity and I is the current flow into the solid. The factor of four is a result of the splitting of the current from each source into the four adjacent quadrants.

If the conductor has anisotropic conductivity components σ_a, σ_b, and σ_c along the geometrical axes a, b, c of the crystal, then the anisotropic problem may be converted into an isotropic situation by the transformation

$$x_i' = x_i(\sigma_m/\sigma_i)^{\frac{1}{2}} \qquad i = a, b, c$$

where

$$\sigma_m = (\sigma_a \sigma_b \sigma_c)^{1/3}$$

and where x_i' is a positional component in the transformed (isotropic) space, x_i' is a positional component in real space and σ_m is now the isotropic conductivity of the transformed solid. This transformation leaves the voltage at corresponding points invariant and requires that equal currents flow through corresponding areas.

We now have the necessary information to derive the apparent conductivity seen in a sample in which the current and voltage contacts to the sample are point contacts rather than line contacts across the face of the sample. The apparent conductivity calculated for current contacts at the corners of a crystal with dimensions L, W, t and voltage contacts symmetrically placed at (x,y) on the face of the sample is

$$\sigma(x,y) = \frac{L}{Wt} \cdot \frac{I}{2V(x,y)}$$

where

$$V(x,y) = \frac{I}{\pi t(\sigma_L \sigma_W)^{\frac{1}{2}}} \sum_{n=-\infty}^{\infty} \ln \frac{\sin^2\left(\frac{\pi x}{2L}\right) + \sinh^2\left[\frac{\pi(y-2nW)}{2L}\right]\left(\frac{\sigma_L}{\sigma_W}\right)^{\frac{1}{2}}}{\cos^2\left(\frac{\pi x}{2L}\right) + \sinh^2\left[\frac{\pi(y-2nW)}{2L}\right]\left(\frac{\sigma_L}{\sigma_W}\right)^{\frac{1}{2}}}$$

and where σ_L and σ_W are the conductivities for the face of the sample. By superposition, the potential when current contacts are symmetrically located at arbitrary positions (A,B) and (A, L-B) in the crystal is

$$V(x,y\colon A,B) = \tfrac{1}{4}[V(x+A,\ y+B) + V(x+A,\ y-B)$$
$$+ V(x-A),\ y+B) + V(x-A,\ y-B)]$$

The results of some example calculations using our experimentally measured values of conductivity on TTF-TCNQ are shown in Fig. 22. It is easy to see that very large errors can be introduced in a conductivity measurement if the contacts are small areas.

Shown in Fig. 23 is a comparison of the experimental results of Schafer et al.[8] obtained with a deliberate misalignment of probes and our calculations with a similar configuration shown. Although we were able to closely match the Schafer et al. results, we were unable to find any combination of probe positions that would reproduce the temperature

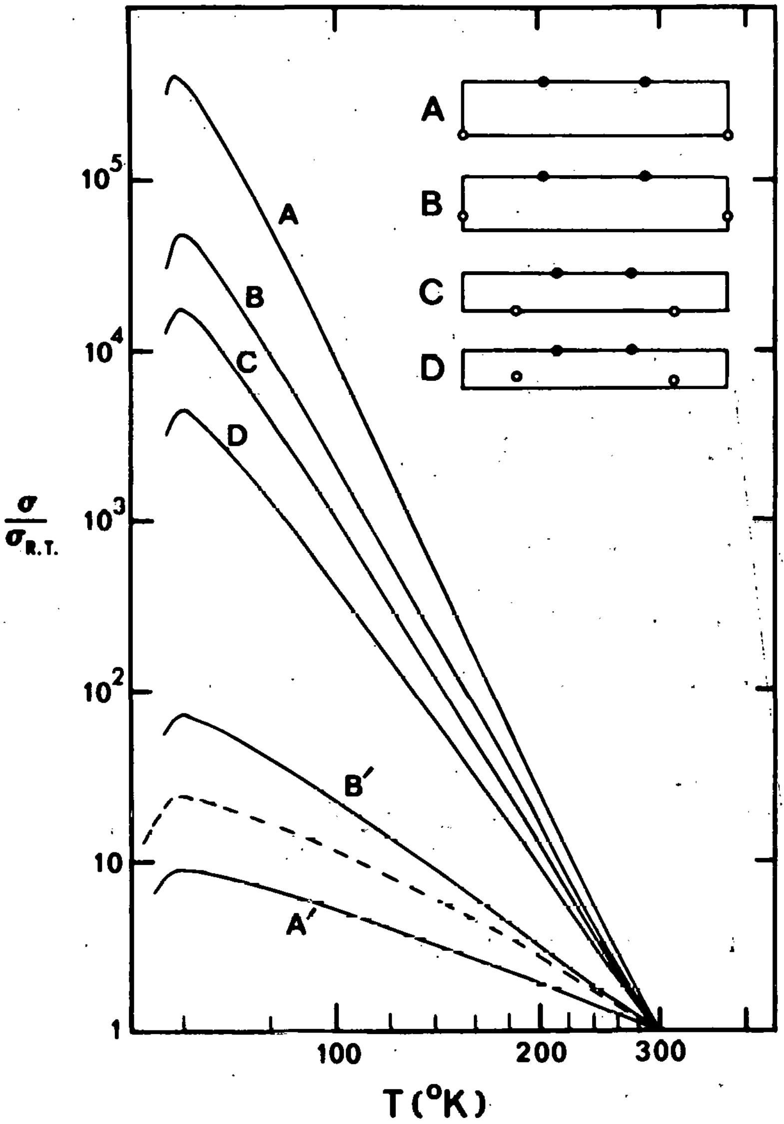

Figure 22. Examples of Apparent Conductivity Calculations.

Current and voltage contacts are represented by open and closed circles, respectively. Width to length ratio is exaggerated by a factor of 2 in the diagrams. The primes refer to equivalent configurations with voltage probes located on the opposite edge of the sample. Also shown, dotted, is our experimentally measured conductivity of TTF-TCNQ.

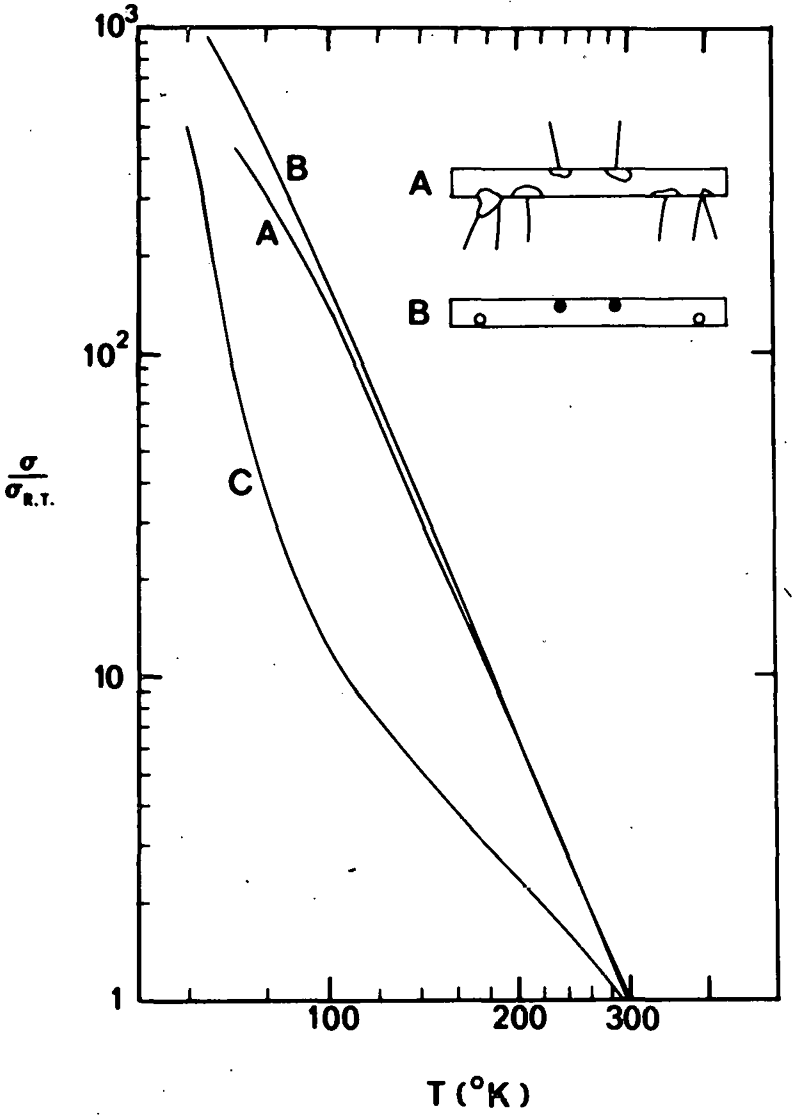

Figure 23. Comparison of Experimental and Calculated High Conductivity Curves for TTF-TCNQ.

Curve A is the experimental results of Schafer et al. (Ref. 8) (replotted). Their sample configuration is shown schematically with the current contacts being the outside contacts on the lower edge, and the voltage contacts being located on the upper edge. Curve B is the result of calculation of apparent conductivity for the similar configuration shown. Curve C is the anomalously high conductivity curve of Coleman et al. (Ref. 7) (replotted).

dependence of high conductivity peak of Coleman et al.[7] we conclude that the extraordinary conductivity curves of Coleman et al. cannot be explained by a simple misalignment of probes.

APPENDIX II

Description of Computer Programs

1. COND: This reduces the experimental conductivity data. Conductivities are calculated from voltage-current ratios. Temperatures are found by interpolation of calibration tables for resistance and thermocouple thermometers.
2. MONT: This reduces the voltage-current ratios obtained in a Montgomery configuration conductivity experiment, giving transverse and longitudinal conductivities.
3. HP: This program calculates apparent conductivities as detailed in Appendix I, using experimentally measured longitudinal and transverse conductivities.
4. LO: Inputs to this program are Lorentzian oscillator parameters. The outputs include a plot of the calculated reflectance to compare with the experimental reflectance and plots of the calculated optical properties when the reflectance fit is deemed adequate.

THIS PAGE
WAS INTENTIONALLY
LEFT BLANK

INTERNAL DISTRIBUTION

1. Biology Library
2-3. Central Research Library
4. ORNL Y-12 Technical Library Document Reference Section
5-6. Laboratory Records Department
7. Laboratory Records, ORNL (RC)
8. ORNL Patent Office
9. J. A. Auxier
10. J. L. Blankenship
11-16. T. A. Callcott
17. R. N. Compton
18. W. R. Garrett
19. C. K. Johnson
20. A. L. McCray
21. H. C. Schweinler
22-41. R. J. Warmack

EXTERNAL DISTRIBUTION

42. A. F. Garito, Department of Physics, University of Pennsylvania, Philadelphia, Pennsylvania 19174
43. G. A. Thomas, Bell Laboratories, Murray Hill, New Jersey 07974
44. J. B. Torrance, IBM Research Center, P. O. Box 218, Yorktown Heights, New York 10598
45. Research and Technical Support Division, ERDA, ORO
46-72. Technical Information Center (TIC)